ORIGINAL PAPER

Propagation and Prediction of Blasting Vibration on Ground Surface Induced by Underground Mining with Comparison to Vibration Inside Rock

Yonggang Gou[1,2] · Lizhen Shi[1] · Xiaofeng Huo[3] · Zhi Yu[3,4] · Yumin Chen[1]

Abstract

Evaluation of ground motion induced by underground blasting is a growing concern due to increased mining of large underground deposits. A numerical analysis is first conducted on the wave propagation characteristics, taking into account geological conditions and ground topography, and it is compared to that resulting from open-pit blasts. Then systemic experiments are conducted at two ore blocks in an underground mine. Predictions are made for peak particle velocity (PPV), frequency, and their combination for ground motions, which are then compared to inside rock vibrations induced by the same ore block blasts. Due to traditional inadequate prediction, the response spectral analysis and the normalized pseudo velocity response spectra (NPVRS) are employed to create a novel approach for illustrating ground motions. The results of numerical calculation and experimental analysis allow for the following conclusions: the wave propagation induced by underground blasting along the ground surface is more complex than that from open-pit blasts; the effect of charge weight on ground vibration decreases with a power factor (n) in the scaling attenuation equation lower than 1/3, as opposed to the typically acceptance of n being 1/2 for open-pit blasts and 1/3 for inside rock vibration induced by underground blasting; the frequency significantly drops from inside rock to ground surface; the NPVRS is a reasonable indicator for quantifying ground motions at specific positions with connecting structural responses, the relative displacement in the concerning frequency range of 5–20 Hz is linearly proportional to ground peak amplitudes.

Highlights

- A systematic experimental work on surface ground motion induced by underground blasting
- Comparison of inside rock and ground vibration from underground blasting
- Decreasing effect of charge weight on ground vibration induced by underground blasting
- Normalized pseudo velocity response spectra (NPVRS) can be simplified as the same at a specific position for effectively predicting ground vibrations

✉ Xiaofeng Huo
huoxiaofeng@gmail.com

1 College of Civil and Transportation Engineering, Hohai University, Nanjing 210098, China

2 Nantong Ocean and Coastal Engineering Research Institute, Hohai University, Nantong 226000, China

3 Zijin School of Geology and Mining, Fuzhou University, Fuzhou 350116, China

4 Oulu Mining School, University of Oulu, 90014 Oulu, Finland

1 Introduction

Ground blast vibrations always cause cosmetic and structural damage and pose a nuisance to residents (Wang et al. 2023). Various prediction models, safety standards and criteria have been proposed to determine the potential for structural damage induced by ground vibrations (Yan et al. 2020). For instance, the scaling law for ground peak particle velocity (PPV) is generally utilized with a power factor of 1/2 or 1/3 (Dowding 1996), the combination of vibration PPV

and frequency content is commonly used in many safety standards to evaluate structural damage, as shown in Fig. 1a (Lu et al. 2012; Dogan et al. 2013; Karadogan et al. 2014). However, these relationships and standards were primarily derived from abundant data and analyses of open-pit blasts. Underground blast-induced ground motions receive less attenuation and comparative analysis due to small amplitudes caused by large stand-off distances from the explosive sources. In recent years, depletion of shallow metal sources, falling ore deposit grades, and environmental protection have increased interest in mining of large deposits underground (Hong et al. 2023). Simultaneously, concerns and complaints have arisen regarding the effects of induced ground blast vibration. These concerns have led mining industries and regulatory agencies to greater interest in the evaluation of ground motions induced by underground blasting.

In contrast to the commonly recognized circumferential wave propagation that occurs around the ground surface due to open-pit blasting (Görgülü et al. 2013), the wave propagation induced by underground explosions is typically assumed to be a spherical or cylindrical form within the rock mass, affected by factors such as charge length, distance, and rock mass properties. As the wave propagates to ground surface, Blair (2015a) combined wave reflection theory with the Heelan model to provide the propagation wave fronts induced by the underground long charge borehole, while the surface waves are neglected due to their computational complexity. Li et al. (2011) conducted a two-dimensional theoretical analysis in an elastic, homogeneous, isotropic half-space rock medium, and they found that surface ground PPVs are influenced by reflected body primary (P-wave) and secondary waves (S-wave) at shorter distances, surface waves become significant as stand-off distances increase. But the calculation of surface waves is based on the differential velocity of two adjacent particles on the ground, which is difficult to correlate with the generating theory of surface waves. Since the theoretical analysis is complex for illustrating propagation characteristics of ground vibrations induced by underground blasting, Gharehgheshlagh and Alipour (2020) monitored 140 underground blast events and found that the induced ground vibration variations differ in diverse sites because of varying field geology conditions and blasting parameters at each site. Some numerical and small-scale experimental results in the depth direction (Gui et al. 2018; Jayasinghe et al. 2019) also demonstrate that the PPV of ground vibration was decreased as the vibration travels from rock to soil. However, our recorded vibrations from inside rock to ground surface in an underground mine show that the PPVs do not necessarily decrease (shown in Fig. 1b), which depends on the specific soft superficial layers (Gou et al. 2023). Jiang et al. (2017) investigated the ground vibration in different topographical zones, such as slopes, mountains or valleys, and found that the PPV and dominant frequency (DF) on the slopes decrease with increasing elevation, rather than exhibiting altitude amplification. These results indicate that the complex propagation characteristics of ground vibrations induced by underground blasts are affected by various factors, which remain controversial.

Anyway, PPV remains a widely used indicator for predicting ground motions produced by underground blasting. Hao et al. (2001) suggested cube-root scaling and site conditions are bases for illustrating induced ground PPVs. Rouse et al. (2020) used the square-root scaling and provided upper-bound regression limits for ground motions from three underground mines. While Ray and Dauji (2019) developed site-specific ground vibration attenuation relationships for a rocky site and proposed that the power factor for the best-fit scaled distance is 0.667 instead of the common values of 1/2 and 1/3. Some attenuation equations were also proposed to obtain a superior prediction of PPV by considering geological properties, such as geological strength index (GSI), rock quality designation (RQD), and soil properties (Kumar et al. 2016, 2020). Tribe et al. (2021) also developed a complex formula based on the dimensional analysis and frequency parameters to improve the prediction of PPVs. Regarding ground motion frequency, Gou et al. (2020) found that the frequencies induced by underground blasting are dispersed when compared to those inside rock, irrespective of DF or average frequency (AF). Similarly, Roy et al. (2016) observed that scattered ground DFs range from 25 to 225 Hz for horizontal distances up to 300 m from underground explosive sources. However, no reasonable attenuation relationship has been proposed. Thus, there is still no consensus on the prediction of ground motions, particularly at frequencies with limited literature available.

The above studies state that there is no consensus on the propagation and prediction of ground motions induced by underground blasting regardless of amplitude and frequency; needless to say the characteristic discrepancies between inside rock and the ground vibrations, as well as comparisons of ground vibrations between underground blast and open-pit blasts. Therefore, based on the inside rock vibrations have been recorded in our previous work (Gou et al. 2020), the wave propagation induced by underground explosives is first analyzed from inside rock to ground surface with considering the influences of geology and topography, then the ground motions induced by blasts at both ore blocks in an underground mine is recorded to analyze and predict PPV, frequency and the characteristics of combination of PPV and frequency with comparison to the inside rock vibration. Finally, a novel approach based on the response spectral analysis is proposed to predict potential damage.
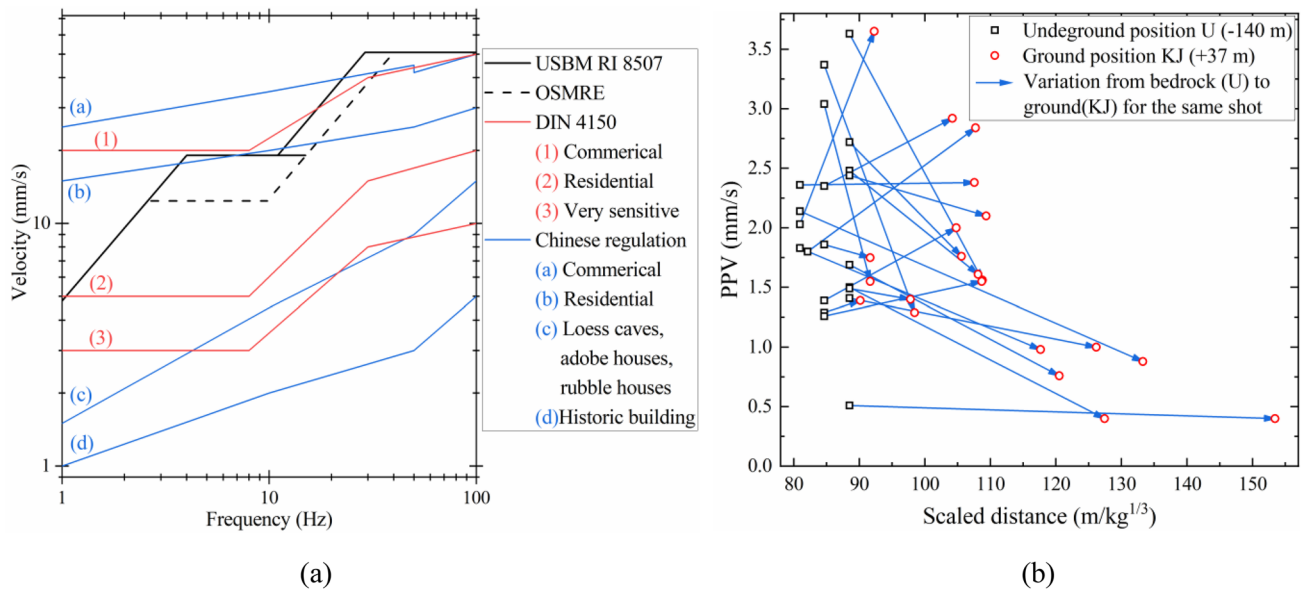
(a)

(b)

Fig. 1 Safety standards and variations of ground vibrations. **a** Four safety standards; **b** PPV variation from bedrock to ground surface at the same ore block (Gou et al. 2023). Noting that the USBM represents the United States Bureau of Mines, OSMRE is Office of Surface Mining, Reclamation Enforcement, and DIN 4150 is the German standards; Chinese safety regulations are also considered since the study was conducted in China

2 Characteristics of Wave Propagation from Underground Explosions

The wave propagation characteristics induced by underground blasting are the foundation to predict ground motions. To date, the theoretical approach is capable of providing an elastic half-space illustration induced by a separate underground incident wave component (Liu et al. 2013), as shown in the right part of Fig. 2 and it mainly focuses on the reflected vibration characteristics without considering surface waves due to the complex calculation of imaginary numbers. The complete incident waveform (including P-wave, SH-wave, and SV-wave) solution considering varying incident angles is located in the exploratory stage. Even if these are works, the practical propagation medium is difficult to be regarded as semi-infinite elasticity (the left part in Fig. 2), there are always soft superficial layers (such as weathered strata, soil layers), various structural planes either large or small, and ground surface topography. The characteristics of ground motions are significantly complicated by these factors, but it is difficult to account for them in theoretical calculations. Therefore, a numerical method is used to further analyze the vibration propagation characteristics (Dai et al. 2019).

A quasi three-dimensional (3D) finite element model is constructed to analyze the variation trend of vibration propagation, this method has been verified as a feasible way to describe blasting wave propagation (Blair 2020, 2023). The model is plotted in Fig. 3 with dimensions of 500 m × 500 m (length × height) and a thickness of element size. The Lagrangian method is employed in LS-DYNA, and the associated governing equations for Lagrangian solids can be referred to Gharehdash et al. (2021) and Hallquist

Fig. 2 Wave propagation from an underground explosion to ground surface
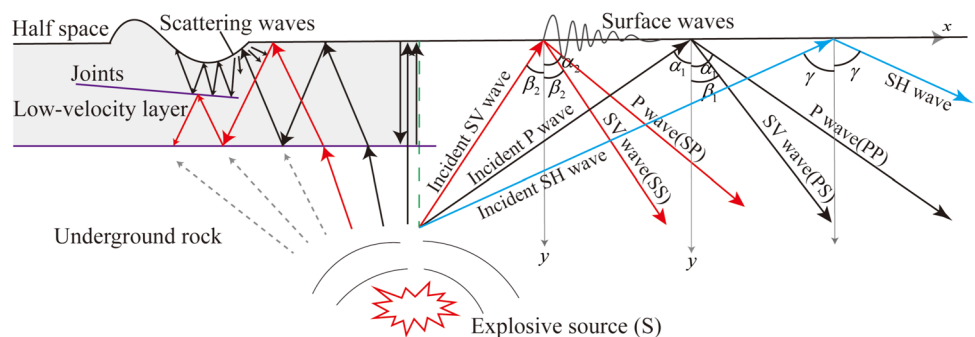
(2006). The numerical cases include: (1) simple half-space rock mass model, in which the point source and long charge explosion are calculated and compared; (2) half-space model with consideration of soft superficial geological conditions, in which two different layer properties are calculated by employing long charge explosion; (3) semi-infinite rock model with long charge explosion and varying terrain, which is shown as the gray dashed line.

The propagation medium is simplified as elastic materials based on limited actual parameters (Blair 2015a, 2023), and the non-reflecting and symmetric boundaries are set as Fig. 3. The involved properties of the rock and both near-surface layers are shown in Table 1 based on the experimental geological investigation in Sect. 2 and our previous paper (Gou et al. 2023).

The borehole is initiated at the bottom end, and the explosive pressure loading on the borehole is calculated using Eq. (1) (Blair 2015b).

$$S(t) = P_{VN}(e\gamma/n)^n \left\{ 1 - \left[1 + \frac{1000}{\sqrt{m}} \left(\frac{\gamma t}{n} \right)^m \right]^{-1} \right\} H(t) t^n e^{-\gamma t}$$

$$(1)$$

where P_{VN} is the (Von Neumann) borehole pressure at the detonation front produced by the explosion, $H(t)$ is the Heaviside unit step function, γ is a pressure decay parameter, n is an integer, and m is an adjustable parameter dependent upon the rise time of the pressure–time history up to its maximum value. The values of $P_{VN} = 1.8 GPa, \gamma = 9000$, $n = 5$, and $m = 5$ based on the general selected values (Blair 2007, 2015b), which are widely used in blast vibration simulation (Ainalis et al. 2016; Yang et al. 2019). It is important to note that the blast loading parameters may have certain differences from practical explosives, but they are sufficient to observe the overall variation trend of wave propagation for given blasting conditions. Furthermore, even if the simulation is verified, a specific numerical condition is also difficult to provide guidance for the subsequent study of the scatter records and statistical laws.

Since the element size for wave propagation problems should be shorter than 1/8–1/10 of the wavelength (Kuhlmeyer and Lysmer 1973), the element size is finally determined to be 0.714 m depending on the pressure frequency, resulting in a total of 0.5 million elements. The numerical time step should be larger than 0.1 times of the characteristic time, which is based on the Nyquist law and calculated as 0.1275 ms. As a result, the time step is determined to be 0.05 ms.

Consequently, both point source and long charge borehole cases with a length of 50 m are first conducted. As the wave propagation to the ground surface is similar in both cases with considerable distances, only the long explosive source case with a horizontal ground surface is shown in Fig. 4a. Next, the two different geological layer cases are conducted and shown in Fig. 4b, followed by the varying terrain case, which is further illustrated in Fig. 4c. Their velocity legends are consistent, ranging from 0 to 6 cm/s.

Figure 4a displays the reflected waves of PP (reflected P-wave from incident P-wave), PS, SP, SS and R-waves are normally shown on the ground surface, and R-waves are only generated from the S-wave component. Additionally, there are some follow-up waves at the time of 154 ms resulting from the left boundary of the model. In both cases shown in Fig. 4b, multiple reflection waves present at the geological layer boundaries and the ground surface, but in the case of differing layers case_2, the wave does not reach the ground
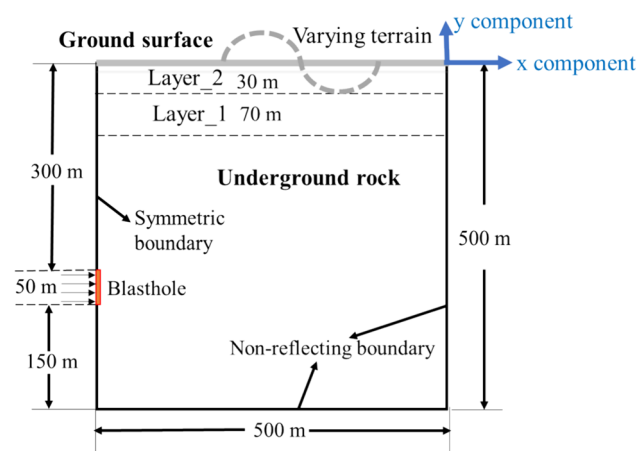

Fig. 3 Configuration of numerical models for underground blasting with consideration of soft superficial layers and varying terrain

Table 1 Properties of the rock and near-surface layers adopted in the numerical model

Material type	Density (kg/m³)	Elastic modulus (GPa)	Poisson's ratio	Cp/Cs
Rock	2700	69.2	0.26	5600/3189
Near-surface layers (case 1: Layer_1/Layer2)	2160/1700	45.2/22.0	0.32/0.40	Cp: 5472/5266 Cs: 2815/2150
Near-surface layers (case 2: Lyer_1/Layer_2)	2429/1959	5.00/0.22	0.30/0.36	Cp: 1665/434 Cs: 890/202

Case 2 represents the condition of weathered rock and soil layers upon underground rock

surface at 154 ms due to its small propagation velocity. These wave components are intricately mixed and propagate in near-surface low-velocity layers, even forming a channeling effect in the case_2 owing to the remarkable variation of geological conditions. Thus, it is difficult to distinguish each wave propagation trajectory along layer_1 and layer_2. Considering the changing ground terrain in Fig. 4c, scattering waves are generated, forming many wavefronts with different propagation directions in the medium. These cases indicate that near-surface low-velocity layers and ground topographical conditions can produce complex characteristics of ground vibration propagation from underground blasting. Note that the constant velocity range in these contours is used because the velocity changes over time in each case, it is difficult to illustrate vibration quantitative changes from inside rock to the ground surface. Therefore, the velocity amplitude variation inside the rock and on the ground surface for the five cases is further shown in Fig. 5. The monitoring line within the rock is indicated by dotted

blue lines in Fig. 4, which is along the depth and parallel to the borehole at a distance of 100 m. It should be noted that the point source case is not shown inside rock due to its low velocity, the varying topographic case is not plotted as it performs similarly to the long borehole case, which is also supported by the ground vibration performance.

Inside rock, the highest velocity amplitude appears at a slightly upper position of the explosive source due to bottom detonation and upper Mach waves, as shown in the left part of Fig. 5. The amplitude then attenuates with decreasing depth, but is magnified after propagating through the upper layers, particularly in the differing layers_1 case. This indicates that gradually decreasing layer properties would create a higher ground magnification effect, instead of a significant decline in properties. Thus, near-surface low-velocity layers are not necessary to reduce ground PPVs for blasting vibration. Moreover, sudden increases in amplitudes are also present at both layer boundaries.
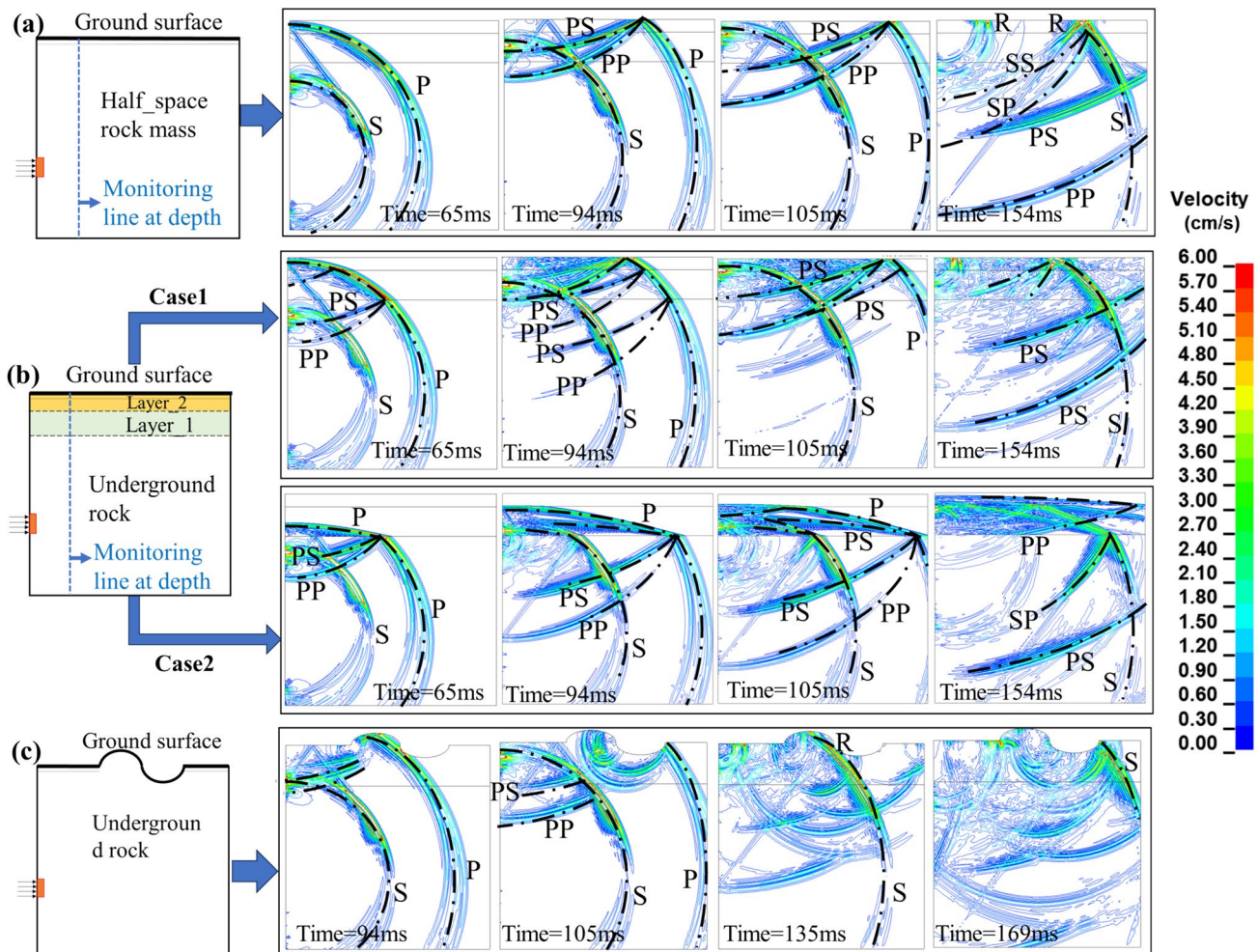

Fig. 4 Wave propagation of three different cases. **a** a simple half-space rock mass model with a long charge explosive source; **b** both half-space models with consideration of near-surface layer properties; and **c** a semi-infinite rock model that considers varying topography

Fig. 5 Velocity amplitude variation inside rock (along the depth direction) and on the ground surface for both x- and y- components (as marked in Fig. 3). The ground surface is set to be at a depth of 0 m for the vibration inside rock, and negative depth is used to distinguish it from horizontal distance on the ground
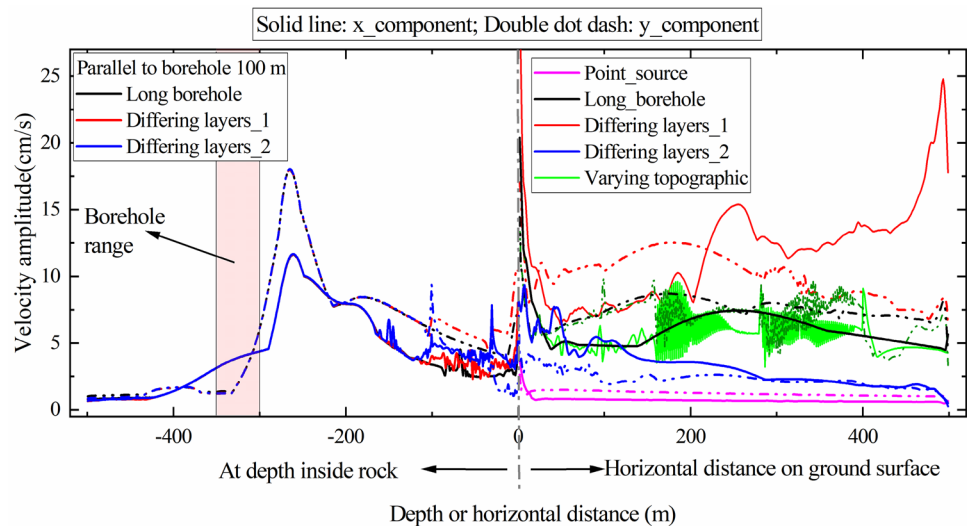
Along the ground surface, the velocity amplitudes attenuate complex with varying blasting conditions, except for the simple point source case. The attenuation curve of the long borehole case fluctuates slightly with varying horizontal distance due to Mach-wave effects, while the varying terrain case presents amplitude oscillations in the canyon and mountain zones based on the long borehole case. When considering geological variation, the amplitude in the differing layers_1 case increases significantly, whereas the differing layers_2 case produces lower attenuation curves. Additionally, the high amplitude at a distance of 500 m is caused by the model boundary.

Furthermore, a comparison of ground amplitude attenuation is made for underground and open-pit blasts with the same charge length 50 m and blasthole condition. The open-pit model is established in Fig. 6a, the comparison of ground velocity amplitudes in both components is shown in Fig. 6b. It states that the ground amplitude of open-pit blasting attenuates at a faster rate than that induced by underground blasts as horizontal distance increases, without considering both amplitude differences.

The above analyses of wave propagation and attenuation show that compared to surface blasts, underground blasting produces complicated vibration attenuation characteristics inside rock and on the ground surface, especially with influences of near-surface geological conditions and ground topography. In practice, the propagation medium consists of even more complex geological layers and discontinuities, making it difficult to view geological layers and varying ground surfaces as regular shapes. Furthermore, the numerical method only describes the pattern of vibration variation, and it is also challenging to accurately depict the practical vibration variation in a complex three-dimensional (3D) medium. Therefore, on-site blasting experiments and monitoring were conducted to directly explore the characteristics of ground motion variation.

3 Description of the Experimental Details

3.1 Site Description and Geology

The experiments were conducted in the Shaxi underground copper mine. There are two main ore blocks shown in Fig. 7: Tongquanshan (TQS) and Fengtaishan (FTS). Both ore blocks adopt the bottom-up mining sequence. According to exhaustive mine geological survey, both ore blocks are located in similar geology with no significant faults or fissures due to porphyritic magmatism, except for the upper weathered strata and the Quaternary soil layer. Figure 8 provides geological information at a depth of 200 m, including the weathering crusts, which vary from 20 to 100 m. Boring logs revealed that the weathered crust contains abundant fractures and joints, as well as disintegrated kaolinized cores (Gou et al. 2023). The rock quality is poor with core loss during drilling. RQD ranges from 3 to 27% with statistical averages of 11% and 10% at FTS and TQS, respectively. According to the classification of weathered rocks for engineering purposes (Dearman 1995; Ietto et al. 2018), the weathered crust falls under classes V (completely weathered) and IV (highly weathered). The upper Quaternary soil layer consists of sand, clay and gravel, and the soil thickness ranges from 0 to 35 m as shown in Fig. 8. The ground surface geology associated with the monitoring zone is shown in the right of Fig. 7, which shows that the Quaternary covers a large area at TQS whereas many old strata are exposed at FTS.
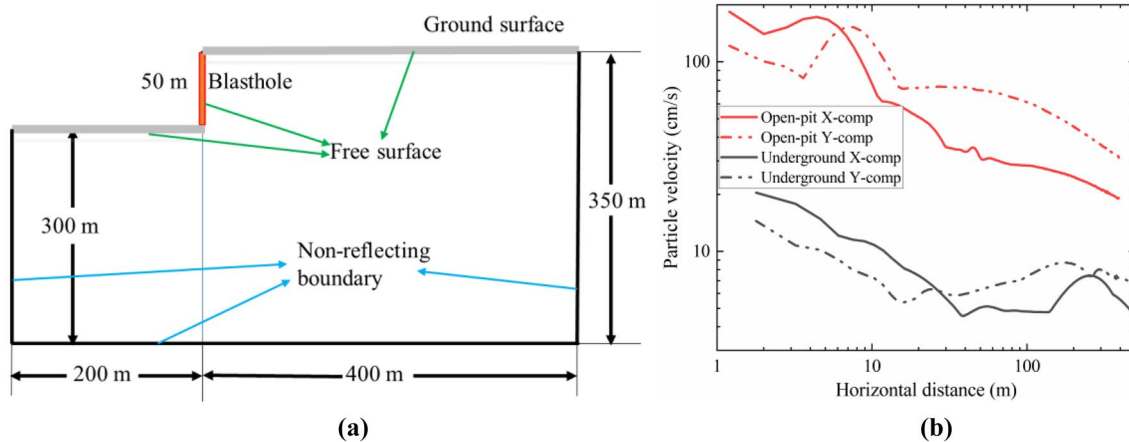
Fig. 6 Comparison of ground velocity amplitude attenuation between underground and open-pit blasts using the same explosive source conditions. **a** The open-pit blast model; **b** The comparison of ground particle velocities
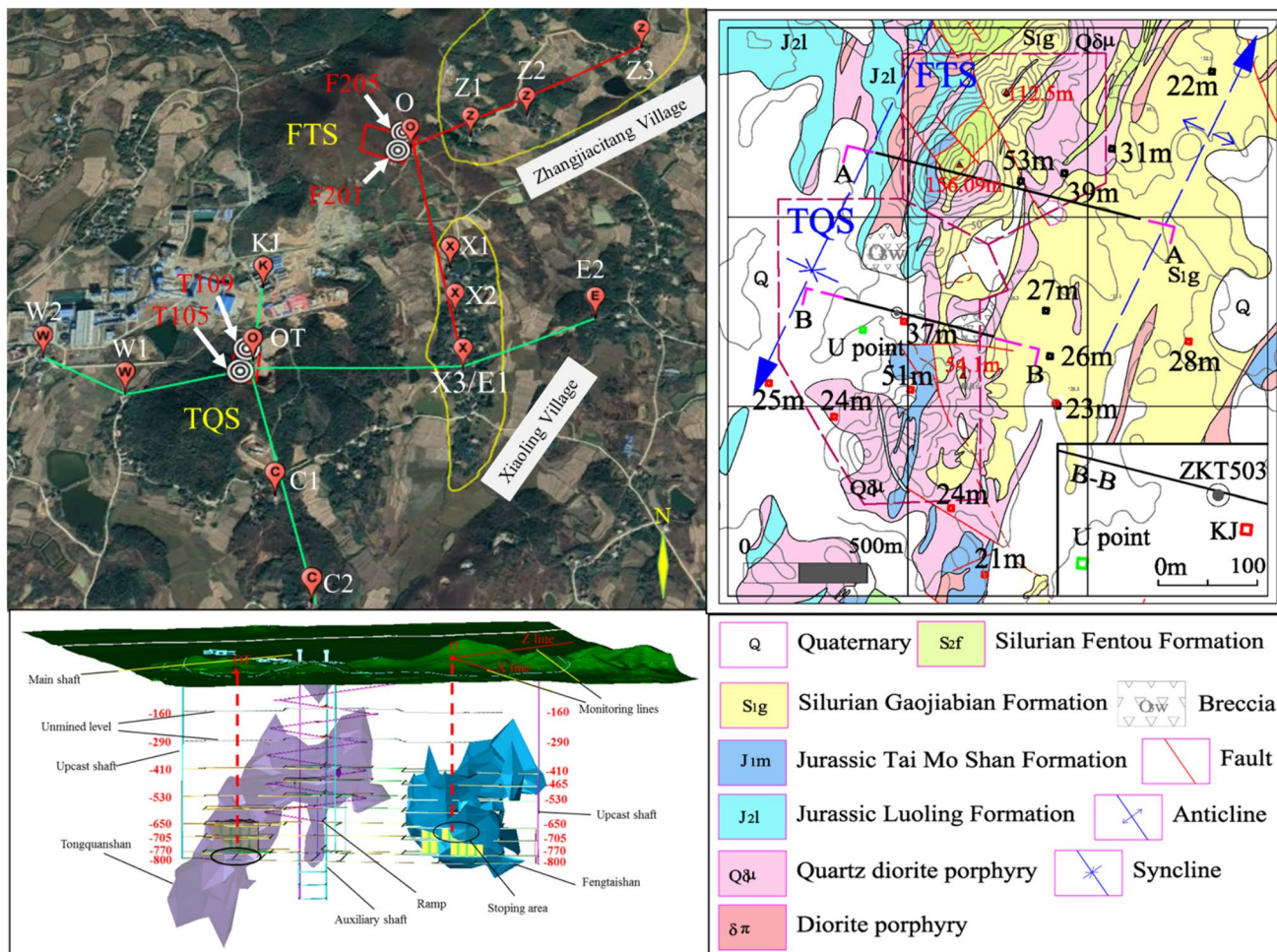

Fig. 7 Configuration and geological view of the experimental site and the ground monitoring stations in the Shaxi underground mine, the boundary of the two ore blocks is surrounded by dark red dashed lines in the geological plan view
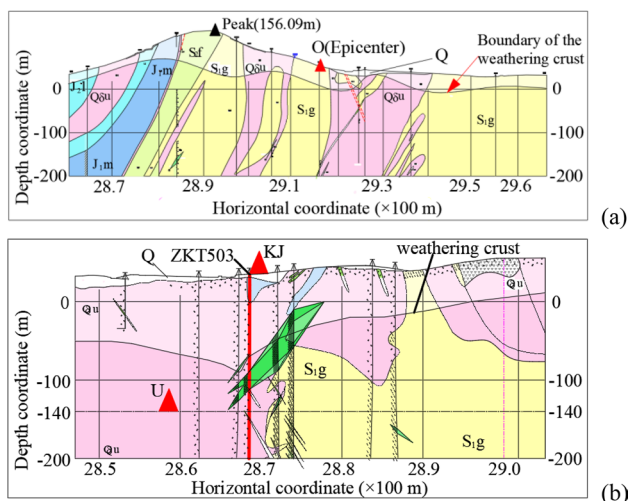
Fig. 8 Geological profile at both ore blocks. **a** Geological profile A-A at FTS; **b** Geological profile B-B at TQS

3.2 Experimental design in underground mine

The experiments were conducted in two FTS stopes (F201 and F205) at the level of -650~-705 m and two TQS stopes (T105 and T109) at the level of -705~-770 m. The size of these stopes is 80×30×60 m (length×width×height) and are mined using the large-diameter long-hole method combined with vertical crater retreat slotting and lateral caving. The experimental full-scale blast geometry is shown in Fig. 9a and is the same for both FTS and TQS. The experimental blasts were conducted in the lateral zone with both spacing and burden of 3.0 m. Due to supporting pillars between rock drilling chambers, inclined holes were arranged to replace vertical holes in several columns. The maximum borehole lengths were 44.2 m at the FTS stopes and 55.1 m at the TQS stopes. The boreholes were conventionally detonated row by row, following the specific detonation sequences were in an experimental blast as shown in Fig. 9b. The design delay interval was 50 ms based on the available detonators in this mine, and the interval is affected by delay errors of 6–10%.

The explosive placement is also shown in Fig. 9c. The emulsion explosive was placed at a length of 0.4 m and a weight of 9 kg. Double detonating cords were laid along the full length of each borehole, and double detonators were attached to the detonating cords, connecting these detonating fuses to the underground initiation network. The charge patterns of the production holes differed from those of the perimeter holes. Charge patterns in several holes were also adjusted to achieve the designed maximum charge per delay. The maximum charge per delay at the FTS for each blast was uniformly distributed from 198 to 860 kg with an approximate interval of 50 kg, while at the TQS it varied from 158 to 711 kg. The total weight of explosives in a blast round (generally no more than two rows) varied from 1122 to 4986 kg.

3.3 Monitoring of Ground Vibration

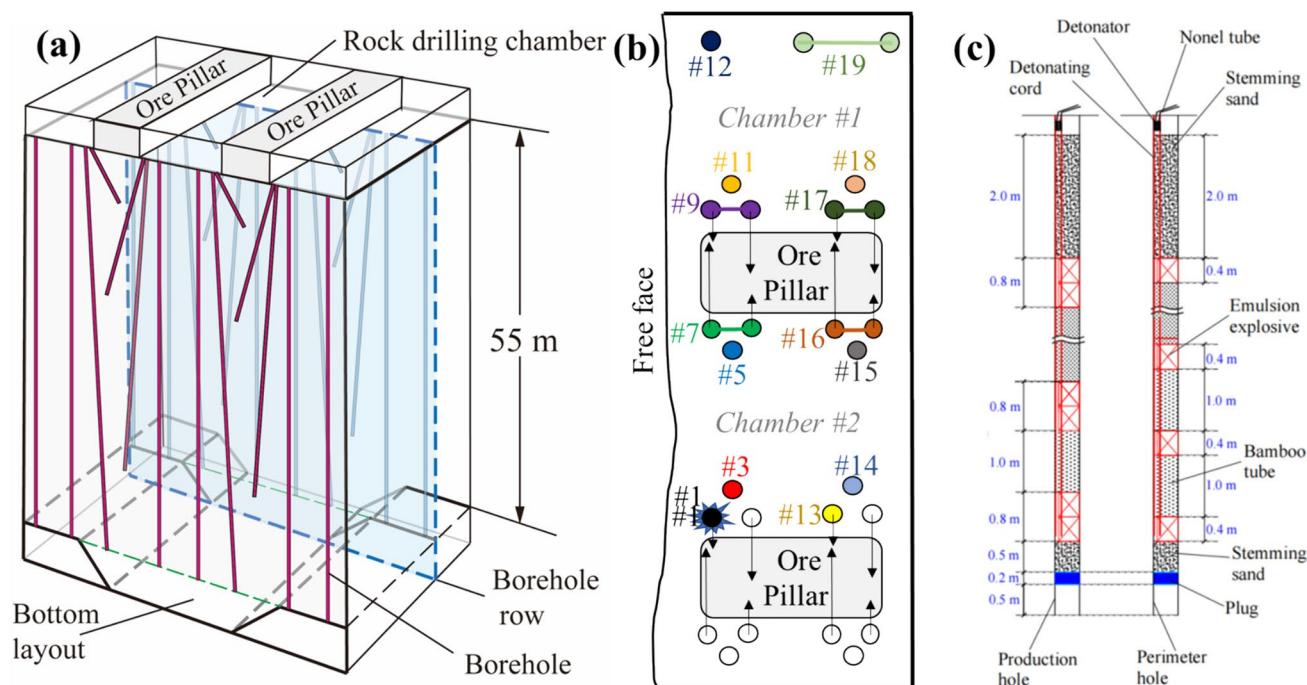As shown in Fig. 7, ground motions were measured at 15 different locations; 7 over FTS for 4 months, including

Fig. 9 The hole layout and charge patterns for lateral blast in the experimental stopes at TQS

point O located near the epicenter position, points Z1, Z2, Z3 located in the Zhangjiacitang Village (labeled as the monitoring line Z), points X1, X2, X3 located in the Xiaoling Village (labeled as the monitoring line X). Then 8 over TQS for 3 months, including OT located at the epicenter, point KJ located at the foundation of an office building (Kuangjian Department), points E1, E2 located in the eastern village, points C1, C2 located in the center (or middle) village, and points W1, W2 located in the western village. These monitoring sites were located in the neighboring villages and on concrete floors adjacent to load-bearing walls of houses, except for O and OT located at two quarries where soil has been removed. In addition, a station (U) was placed on the mine ramp at level -140 m at TQS as shown in Fig. 8b, for comparison with the ground motions. It is located approximately 167 horizontal meters away from location KJ. Table 2 lists the elevations and distances from the stopes for each location. These offsets result in direct distances between the blast sources and ground monitoring stations of 725.9 to 1177.9 m at FTS, and 784.4 to 1342.5 m at TQS except for U.

At each station, the NUBOX-8016 Monitor recorded the longitudinal (L), transverse (T) and vertical (V) components with electromagnetic geophones. The system is capable of measuring particle velocities ranging from 0.0047 to 35 cm/s with flat responses between 4.5 and 350 Hz at 5000 samples per second. A total of 169 ground motions were recorded from 30 shots at FTS, and 118 from 26 shots at TQS. Some data were not recorded due to low amplitude, which did not trigger the vibration sensors. This was particularly evident at the TQS ore block.

4 Results and Prediction of Ground Vibration with Comparison to Vibration Inside Rock

4.1 PPV Only of Ground Motions

4.1.1 Comparison of PPV Attenuation Between Ground and Inside Rock

The measured data along the depth inside rock were recorded from six positions and illustrated in our previous study (Gou et al. 2020), the recorded blasts were located at the same level of -705 ~ -770 m of the TQS. In Fig. 10, these data along with the measured ground PPVs at the TQS are illustrated to compare their differences. Some of the blasts triggered remote monitoring positions at the FTS, and these data are also included. Furthermore, the Theil-Sen regression method, a nonparametric approach, is utilized to derive reasonable regression curves based on blast vibration characteristics. The 1/3 and 1/2 power-law scaling attenuation equations are also shown for the inside rock and ground vibrations, respectively.

The fitting equations in Fig. 10 state that the square root scaled distance produces a higher fit coefficient (R^2) for the surface ground PPVs, while the PPVs inside rock have similar performance with both power laws. Thus, the square root scaled distance is employed to plot the fit lines. From inside rock to the ground surface, the PPVs have a negligible change with a slight declination of the attenuation slope. This indicates that the attenuation trend of the ground PPVs would continue to that of the PPVs inside rock. However, the low fitting coefficient of the ground motions, also the similar performance at the FTS shown

Table 2 Elevations and horizontal distances from the experimental stopes at both ore blocks

Station (FTS)	Elevation (m)	Horizontal distance (m)		Station (TQS)	Elevation (m)	Horizontal distance (m)	
		F201	F205			T105	T109
O	53	63	36	OT	51	75	26
Z1	39	259	224	KJ	37	350	268
Z2	31	472	426	E1	23	677	662
Z3	22	988	931	E2	28	1106	1078
X1	27	487	554	C1	24	433	507
X2	26	672	746	C2	21	798	869
X3	23	866	951	W1	24	352	386
				W2	25	623	629
				U	− 140	345	285

(a) At the FTS, the elevations of the blast centers in both stopes were assumed to be -672 m; while at the TQS, the elevations were − 733 m. (b) Horizontal distances were calculated from both stope centers, and the distance associated with each blast was obtained from the respective blast center
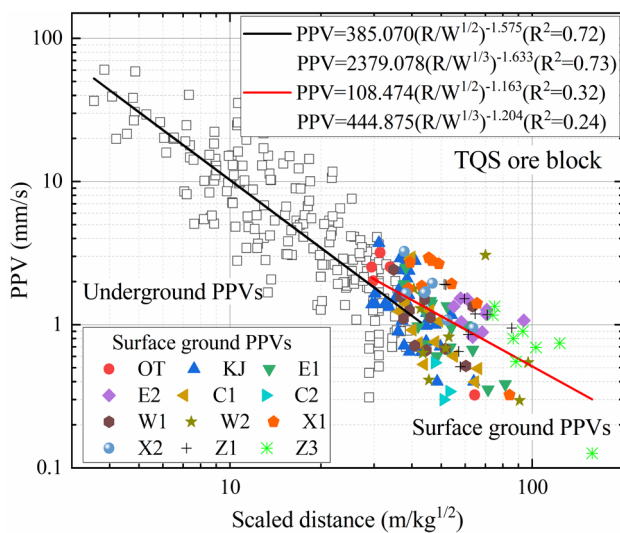
Fig. 10 Comparison of PPVs between inside rock and surface ground at TQS

in Eq. (2), raises a doubt whether the square root scaled distance is reasonable for ground motions.

$$PPV = 319.103\left(R/W^{1/2}\right)^{-1.437}\left(R^2 = 0.33\right)$$
$$PPV = 9160.138\left(R/W^{1/3}\right)^{-1.833}\left(R^2 = 0.36\right) \quad (2)$$

where W is the maximum charge weight per delay, R is the direct distance from explosive sources.

Since each blast has a constant explosion source condition for multiple monitoring stations, only the stand-off distance of the monitoring location varies without considering geological influence. Thus, the PPV attenuation curves for 10 shots at block FTS are shown separately in Fig. 11a. It shows that the PPV does not decrease uniformly with increasing distance for any one shot, regardless of the single delay shot and production shots. This is due to changing geological conditions at different positions. In addition, amplitudes vary from shot to shot due to differences in shot design and relief. For example, the 432 kg case has higher PPVs resulting from the enormous burden, and the 860 kg case has lower PPVs was derived from overbreak of the last blast. To eliminate the effects of the charge weight and related factors, three single-delay shots were further designed with the same 860 kg charge weight at the same FTS stope, the measured PPVs varied with distance (R) along the X line (i.e., O, X1, X2, and X3) and Z line (O, Z1, Z2, and Z3) are plotted in Fig. 11b.

As depicted in Fig. 11b, three shots exhibit comparable results in the X and Z lines. The PPV decreases consistently in the X line, while an irregular decline is observed in the Z line. According to Fig. 7 illustrates that the locations in X line share the same surface geologic strata, while the

geology varies in Z line, the irregular decline in Z line is attributed to varying geological conditions of the monitoring locations. Thus, to better predict the PPV attenuation, it is essential to examine the geological impact on ground motions, particularly the shallow site geological conditions.

4.1.2 Effect of Geological Conditions on Ground PPVs

Since the geological condition is constant at a particular monitoring point, the PPV attenuation at each position is analyzed separately. The general attenuation equation is employed based on no consensus is achieved for the charge weight effect and power laws of scaled distance as:

$$PPV = kW^aR^{-b} = k(R/W^n)^{-b} \quad (3)$$

where k, a, b, n are constants determined by measured data, and n equals to a/b. Regarding charge weight W, some studies in the belief that ground PPVs in the far-field possibly depend on the total charge weight based on the ground waveform period and duration are much longer than the employed maximum delay-time in underground blasting (Blair 1990; Venkatesh 2005), while Blair (2004) proposed that the mean charge weight should be more reasonable to substitute for W. Regarding distance, some researchers proposed that the horizontal distance may be more reasonable for ground vibrations due to the dominant role of surface waves (Lv et al. 2023).

Firstly, the grey relation analysis (GRA) is utilized to investigate the sensitivity between these parameters and PPV, including distance parameters (direct distance, horizontal distance), charge weight parameters (maximum charge weight per delay, total charge weight, mean charge weight). However, these correlation between these parameters and PPV was similar, with an average correlation ranging from 0.742 to 0.773. Then these parameters are investigated by employing Eq. (3), the fitting coefficients (R^2) for each position are depicted as curves in Fig. 12.

The R^2 curves in Fig. 12 demonstrate that the total charge weight and mean charge weight have relatively poor fitting performance for ground PPVs, and both horizontal and direct distances exhibit better and similar fitting performance with using the maximum charge weight, except for positions E1, W1, and W2. Then the power law parameter n is calculated and plotted as bars for both well-performing cases. It can be observed that the n (or absolute value) induced by direct distance is either less than 1/3 or approaching to 1/3 in 11 out of 13 locations, and the n-value induced by horizontal distance is either less than 1/3 or approaching to 1/3 in 10 out of 13 locations. If the abnormally negative values and excessively high values of n are removed, the n values would be closer to 1/6, as proposed in our preceding study (Gou et al. 2020). This statement challenges the widely accepted
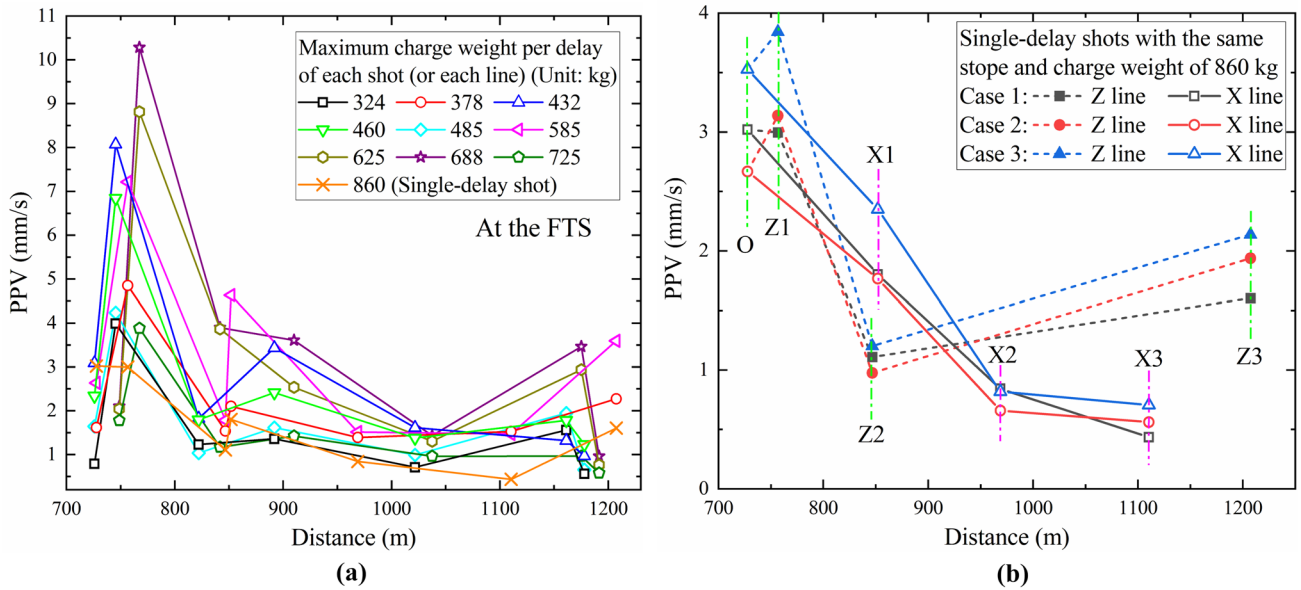
Fig. 11 **a** PPV variations of 10 shots at the FTS. Each line represents a single shot with 7 FTS monitoring positions, while these stations have been rearranged according to their distance from the explosion source; **b** attenuation of three single-delay shots in the X and Z lines with the same stope and charge weight

view that the degree 1/3 can be used for considerable distances when a cylindrical charge can be treated as spherical (Dowding 1996). The vibration propagation from inside rock to the ground surface means that the transformation of inside spherical waves to surface waves, which would potentially result in a coefficient of $1/3 \times 1/2$ as the degree 1/6, corresponding to a decrease in the influence of W compared to n approaches 1/3 inside rock. Nevertheless, this statistical illustration requires further verification through additional ground motions. Thus, the power factor of 1/3 is still used here as a compromise to depict ground vibration attenuation at each position in Fig. 13, the direct distance is employed because the horizontal distance case would easily produce more abnormally negative values of n, such as X2, E2, W2.

Figure 13 shows that there is a difference of attenuation trends between X3 and E1, despite being at the same ground position. This indicates that vibration attenuation differs from ore blocks, even when the site geological condition is constant. This discrepancy could be attributed to differences in propagating paths and underground rock properties. Thus, both ore blocks are illustrated separately.

At FTS, the attenuation slopes are close, ranging from − 1.634 to − 2.160, except for position O (-2.918), but the intercept varies significantly. For example, the PPV level at O is the lowest, while at Z1 is the highest, despite a horizontal distance of only 173 m between the two positions. These indicate that geology primarily impacts amplitude levels rather than attenuation slopes. Although position O is located at the outcrop, its lowest PPV level may be

affected by the topographic conditions. This is due to the mountain peak of FTS, which can generate low amplitudes based on the amplitude complex variation shown in Fig. 5.

At TQS, position OT at the outcrop also presents scattered data, despite limited data recordings. At the other positions, the ground attenuation slopes are distributed over a relatively wide range from − 2.395 to − 3.349,
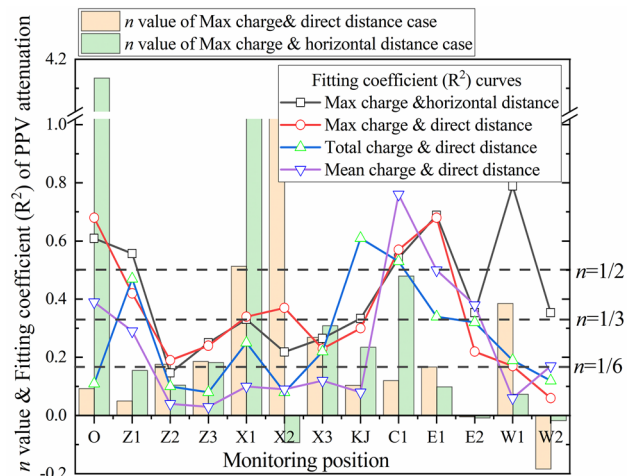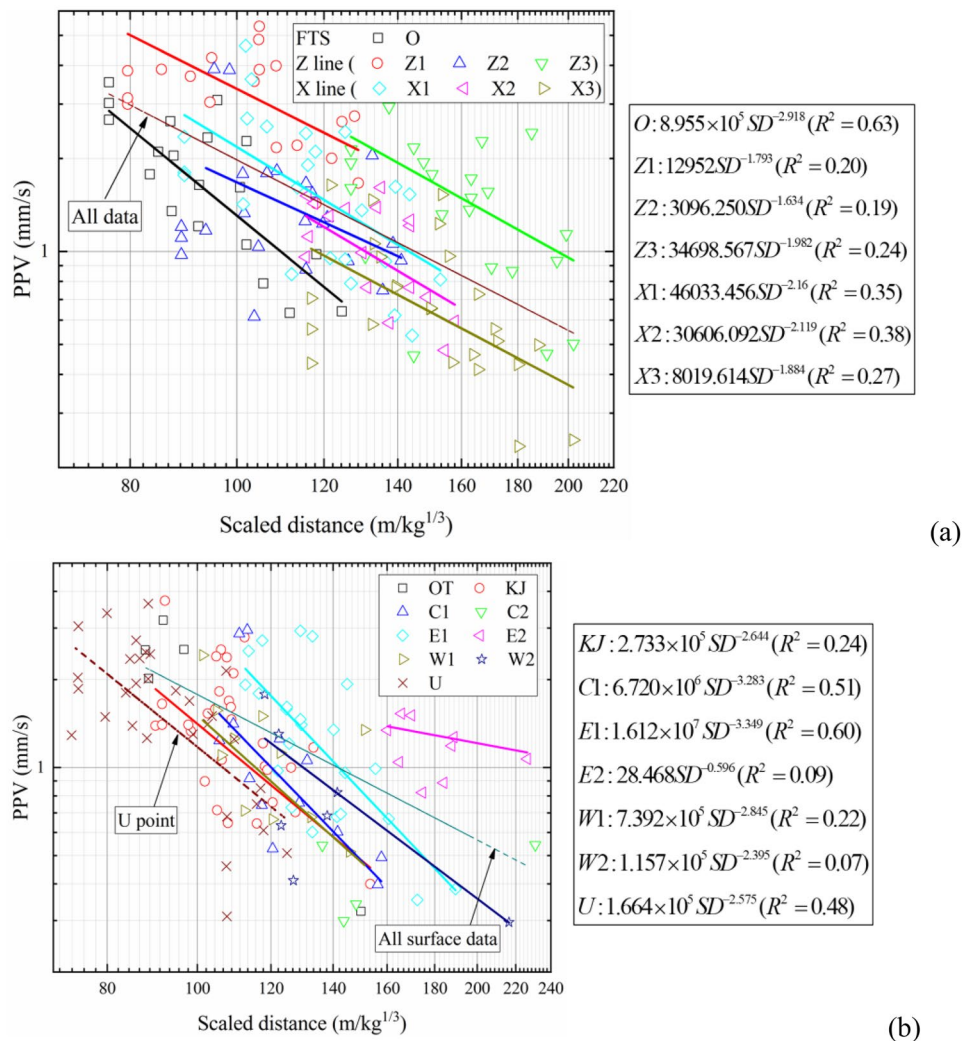

Fig. 12 Parameters of n and fitting coefficient (R^2) at each ground position for different parameter combinations of charge weight and distance. Noting that Max charge represents the maximum charge weight per delay

Fig. 13 PPV attenuation at each position of FTS (**a**) and TQS (**b**), respectively

$$O: 8.955 \times 10^5 \, SD^{-2.918} (R^2 = 0.63)$$
$$Z1: 12952 \, SD^{-1.793} (R^2 = 0.20)$$
$$Z2: 3096.250 \, SD^{-1.634} (R^2 = 0.19)$$
$$Z3: 34698.567 \, SD^{-1.982} (R^2 = 0.24)$$
$$X1: 46033.456 \, SD^{-2.16} (R^2 = 0.35)$$
$$X2: 30606.092 \, SD^{-2.119} (R^2 = 0.38)$$
$$X3: 8019.614 \, SD^{-1.884} (R^2 = 0.27)$$

(a)

$$KJ: 2.733 \times 10^5 \, SD^{-2.644} (R^2 = 0.24)$$
$$C1: 6.720 \times 10^6 \, SD^{-3.283} (R^2 = 0.51)$$
$$E1: 1.612 \times 10^7 \, SD^{-3.349} (R^2 = 0.60)$$
$$E2: 28.468 \, SD^{-0.596} (R^2 = 0.09)$$
$$W1: 7.392 \times 10^5 \, SD^{-2.845} (R^2 = 0.22)$$
$$W2: 1.157 \times 10^5 \, SD^{-2.395} (R^2 = 0.07)$$
$$U: 1.664 \times 10^5 \, SD^{-2.575} (R^2 = 0.48)$$

(b)

with the exception of position E2 due to the scattering data. Compared to the inside rock position U, there is an insignificant change in attenuation slopes, even at position KJ that is the closet ground position on the horizontal projection plane, even though there is a 3.3 m soil layer over the weathered rock between KJ and U. This indicates that near-surface low-velocity layers have minimal impact on ground PPV attenuation rates. Compared to FTS, the overall PPV levels at TQS are lower due to its wide coverage of Quaternary. Additionally, the ground amplitudes at TQS are higher than those at the inside position U, this evidence shows that ground vibration is not necessary to be lower than that inside rock.

However, the R^2 for the equations fitted in Figs. 12 and 13 are still poor, with most of them being less than 0.5. It is difficult to clarify whether this performance results from the soft superficial geological layers (that alter wave propagation paths and complicate ground vibration), or surface waves, or simply experimental scatter over large distances. Since

soft superficial geologic conditions have significant effects on ground horizontal components (Yaghmaei-Sabegh and Rupakhety 2020), Table 3 illustrates the attenuation of PPV in the horizontal (PPVH) and vertical (PPVV) components at FTS ground positions. The PPVH is determined by selecting the larger one of the L and T components. In addition, surface waves will be analyzed separately because it is not included in the effect of geological conditions.

Table 3 shows that position O has the highest R^2 among the observed locations, especially PPVV with an R^2 of 0.77. The n (0.109) of PPVH is roughly twice that of n (0.053) of PPVV, and the b value (8.455) of PPVH is half that of b (17.714). It implies that ground horizontal components are more sensitive to the charge weight, and the horizontal attenuation slope is slower than the vertical component, which is consistent with ground surface waves. However, the other positions have lower fitting coefficients for inferring the attenuation characteristics.

Table 3 Attenuation equations and fitting coefficients for the horizontal and vertical components at FTS

| FTS	PPVH	R^2	PPVV	R^2
O	$1.018 * 10^{22}\left(R/W^{0.109}\right)^{-8.455}$	0.67	$1.852 * 10^{48}\left(R/W^{0.053}\right)^{-17.714}$	0.77
Z1	$1.026 * 10^{31}\left(R/W^{0.065}\right)^{-11.226}$	0.43	$3.970 * 10^{34}\left(R/W^{0.018}\right)^{-12.032}$	0.23
Z2	$6.755 * 10^{23}\left(R/W^{0.037}\right)^{-8.444}$	0.29	$23310.439\left(R/W^{0.189}\right)^{-1.748}$	0.06
Z3	$9.148 * 10^{10}\left(R/W^{0.202}\right)^{-4.264}$	0.32	$5.409 * 10^{5}\left(R/W^{0.241}\right)^{-2.292}$	0.22
X1	$125.223\left(R/W^{0.573}\right)^{-1.312}$	0.34	$154.702\left(R/W^{0.424}\right)^{-1.178}$	0.04
X2	$6.393 * 10^{-10}\left(R/W^{-0.096}\right)^{2.820}$	0.12	$0.070\left(R/W^{-0.507}\right)^{0.195}$	0.08
X3	$1170.126\left(R/W^{0.519}\right)^{-1.500}$	0.24	$1.441 * 10^{11}\left(R/W^{0.083}\right)^{-4.028}$	0.18

4.1.3 Effect of Wave Component on Ground PPV Attenuation

Table 3 analysis implies that the wave component has a significant impact on PPV attenuation due to the dominance of surface waves in the ground horizontal component. Therefore, further investigation is necessary to determine the effect of wave components (body and surface waves) on ground PPV attenuation. As multi-borehole wave superposition induces ground waveforms that are difficult to distinguish the wave components, the waveforms of three single-delay shots (charge weight of 860 kg) at FTS are utilized to uncover the disparities between body waves and surface waves. The surface wave component is identified through the polarization ellipse characteristics of displacement trajectories of Rayleigh waves, and the displacement trajectories of two typical positions O and Z2 are plotted in Fig. 14.

Position O is chosen due to its outcrop condition, and position Z2 is selected because of the abnormally short arrival time difference between P-wave and S-wave compared to the other positions' waveforms.

Figure 14 shows that the R-wave is unequivocal in the vertical plane at position O due to its vertical ellipse trajectory. At position Z2, the first polarization (11.0–18.4 ms) is dominated by the P-wave of the vertical component, followed by an outer ellipse presented in the vertical plane with a major axis that approximates the horizontal direction. This differs from the vertical major axes of R-wave characteristics, half of the ellipse features a reciprocating linear motion along the horizontal L component, while the other half forms an ellipse trajectory. This indicates that the outer trajectory includes not only R-waves, but also Love waves (L-waves) resulting from SH-waves. The early arrival time of surface waves is

Fig. 14 Displacement trajectories at positions O (**a**) and Z2 (**b**)
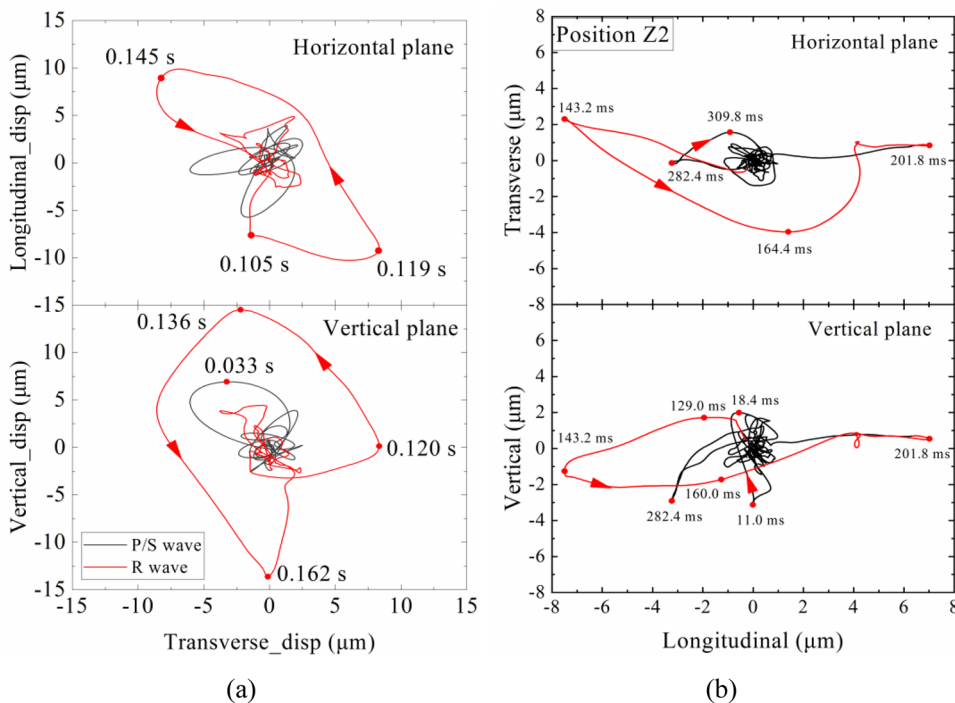
attributed to the velocity of L-waves, which relies on the propagation velocities of layers near the ground and is not necessarily lower than the R-wave velocity. Regarding the amplitude, Fig. 14 illustrates that high-frequency blasting motions produce small ground displacements at a unit level of μm.

Then the peak amplitudes of body and surface waves of the three single-delay shots are presented in Fig. 15, along with the corresponding amplitude ratios of surface waves to body waves. Figure 15 reveals that body waves decline uniformly along both lines, whereas surface waves exhibit erratic changes. The horizontal components show an irregular decrease of surface waves, whereas the vertical component experiences a normal decline. Furthermore, the amplitude ratios of the two horizontal components exhibit significant variation and exceed 1, while the ratios of the vertical components are low (< 1), intensive, and undergo insignificant changes, similar to the outcrop position O produced by similar oscillations in three components. This indicates that site geological conditions would amplify horizontal surface waves, but have little effect on the vertical component.

4.2 Frequency Only of Ground Motions

4.2.1 Comparison of Frequency Attenuation Between Ground and Inside Rock

Apart from the DF determined by the highest peak in the amplitude-frequency spectrum, other indicators such as AF, principle frequency (PF), and mean power frequency (MPF) are also utilized to depict vibration frequency (Wu and Hao 2005; Liu et al. 2022). The AF is susceptible to signal noise, particularly for ground motions with small amplitudes, the PF is not widely used due to its ad-hoc definition for vibration records. The power spectrum of the waveform is more effective at eliminating noise, as indicated by calculation formula Eq. (4). Therefore, in addition to the DF, the MPF is chosen to observe frequency changes. Consequently, DFs and MPFs of both inside rock and ground surface at the TQS ore block are illustrated in Fig. 16a, b, respectively.

$$MPF = \sum_{n=1}^{m} P_n f_n \bigg/ \sum_{n=1}^{m} P_n \qquad (4)$$

where P_n is the power value corresponding to the frequency f_n in a waveform power spectrum.
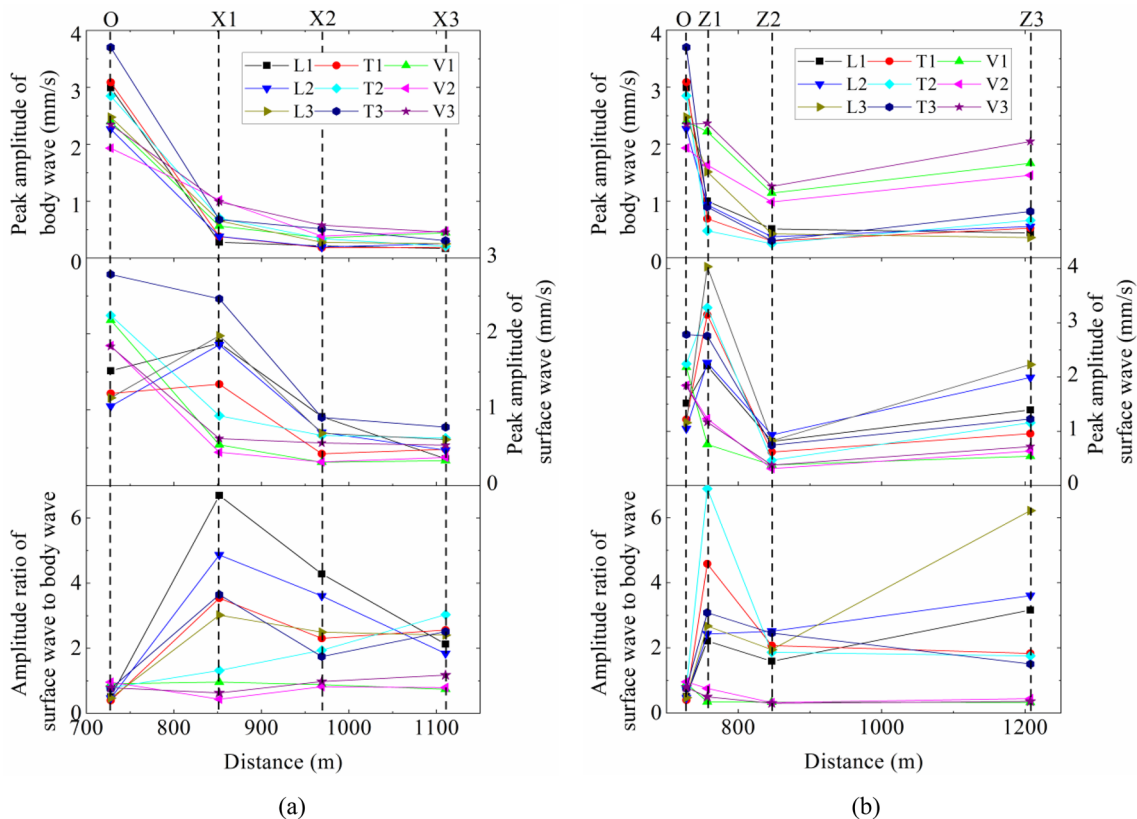

Fig. 15 Peak amplitudes of body waves and surface waves, as well as the amplitude ratios of surface waves to body waves along the X line (**a**) and Z line (**b**), respectively
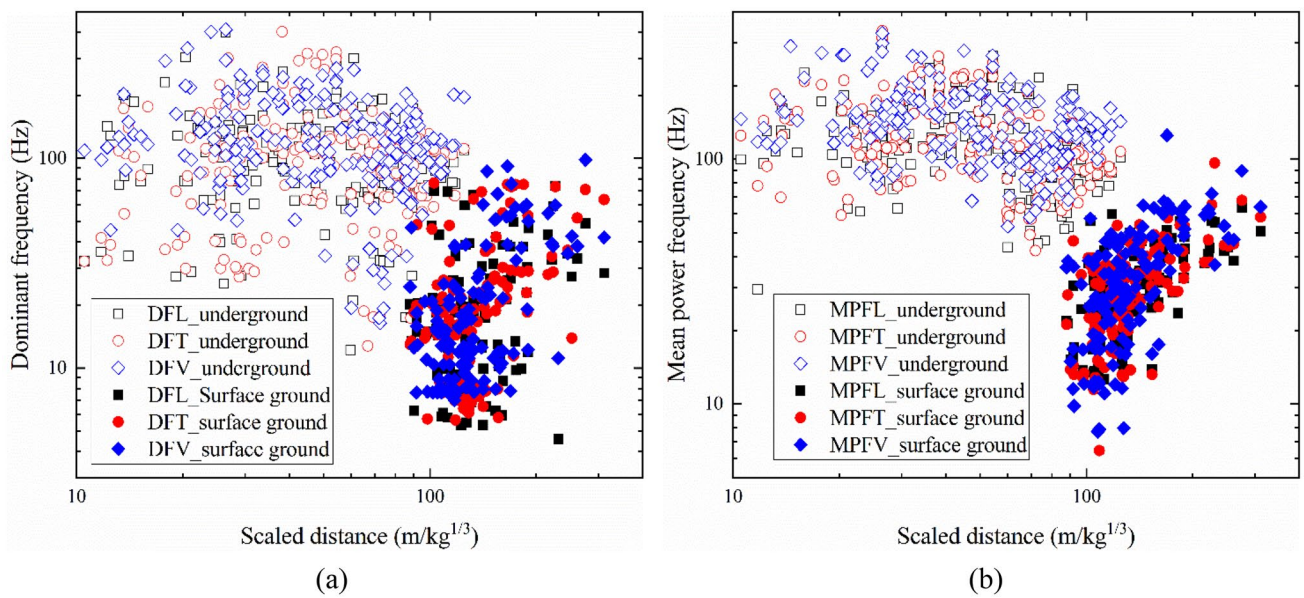
Fig. 16 Comparisons of DFs (**a**) and MPFs (**b**) between inside rock and ground surface at TQS, respectively

Figure 16a shows that the ground DFs and MPFs are significantly lower than those inside the rock, and the trend of the ground motion frequencies also varies from that inside rock. This indicates that the ground surface exerts a substantial effect on vibration frequencies, unlike the PPVs. Based on the following frequency attenuation equations from the dimensionless analysis in Appendix. A and our previous study:

$$f = KW^{-1/3}\left(R \big/ W^{1/3}\right)^{\alpha'} \tag{5}$$

$$f = \left(K \big/ W^{k_1}\right)PPV^{k_2}e^{-bR} \tag{6}$$

where K, k_1, k_2, α are constants, b is a constant to express the damping characteristics of propagation medium. Both equations are employed to investigate attenuation of the DFs and MPFs, and the MPF significantly outperforms the DF. Thus, Table 4 only lists the fitting results of MPFs with calculations for three individual components. It is noticeable that the inside rock vibration is only presented with Eq. (6) because it has been analyzed in our previous study and is optimal to use Eq. (6).

Table 4 demonstrates that Eq. (6) also has a superior fitting performance for ground MPFs, whether all data or three components. The fitting coefficients in Eq. (6) for inside rock and ground are similar, but the constant K values and charge weight power factors decrease significantly for ground vibration. This indicates that the effect of charge weight on blasting vibration decreases from inside rock to the ground surface, which agrees with the PPV analysis that the exponential value of charge weight is less than 1/3 of inside rock vibration. Furthermore, the increasing b values indicate that the propagation medium becomes weaker and softer according to the classification

Table 4 Fitting results for the underground and ground MPFs derived from Eqs. (5), (6)

		Equation (5)	Equation (6)
MPF inside rock	All		$\left(5188.165 \big/ W^{0.572}\right)PPV^{0.178}e^{0.000258R}\left(R^2 = 0.595\right)$
	L		$\left(6179.358 \big/ W^{0.621}\right)PPV^{0.223}e^{2.063\mathrm{e}-5R}\left(R^2 = 0.597\right)$
	T		$\left(7244.531 \big/ W^{0.620}\right)PPV^{0.160}e^{0.00049R}\left(R^2 = 0.560\right)$
	V		$\left(3419.674 \big/ W^{0.488}\right)PPV^{0.152}e^{0.000283R}\left(R^2 = 0.586\right)$
Ground MPF	All	$4.387W^{-1/3}\left(R \big/ W^{1/3}\right)^{0.811}\left(R^2 = 0.326\right)$	$\left(324.212 \big/ W^{0.483}\right)PPV^{0.236}e^{0.000621R}\left(R^2 = 0.496\right)$
	L	$8.696W^{-1/3}\left(R \big/ W^{1/3}\right)^{0.660}\left(R^2 = 0.327\right)$	$\left(189.765 \big/ W^{0.391}\right)PPV^{0.150}e^{0.000532R}\left(R^2 = 0.469\right)$
	T	$3.861W^{-1/3}\left(R \big/ W^{1/3}\right)^{0.833}\left(R^2 = 0.400\right)$	$\left(370.343 \big/ W^{0.506}\right)PPV^{0.194}e^{0.000603R}\left(R^2 = 0.518\right)$
	V	$2.902W^{-1/3}\left(R \big/ W^{1/3}\right)^{0.911}\left(R^2 = 0.318\right)$	$\left(546.693 \big/ W^{0.476}\right)PPV^{0.383}e^{0.000730R}\left(R^2 = 0.597\right)$

of geological materials by damping coefficient (Jedele 2012), and the effect of material damping intensifies.

4.2.2 Effect of Geology and Wave Component on Ground Frequencies

The MPF fitting coefficient is also calculated for each monitoring position, as depicted in Fig. 17. It shows that the fitting coefficients are below 0.45, except for W2 with a value of 0.59. The main reason for this is the insufficient data for each monitoring position, resulting in these values being lower than the overall fitting outcomes listed in Table 4. Moreover, there is no valuable improvement for individual components at each position. These observations indicate that ground motion frequency attenuation is more complex than PPVs.

On the other hand, there are different PPV outcomes between body waves and surface waves, so the DFs of these waves in lines X and Z are shown in Fig. 18. It is noteworthy that MPF, the average parameter linked with the entire waveform, is not considered. The results show that the DFs of body waves exceed those of surface waves. In the line X, the frequencies of body waves decrease consistently, while the frequencies of surface waves undergo insignificant changes due to comparable geological conditions of the site. While in the line Z, the frequencies of body waves display significant variations, and the frequencies of surface waves remain relatively stable. Thus, site geological conditions have a greater impact on body wave frequencies.
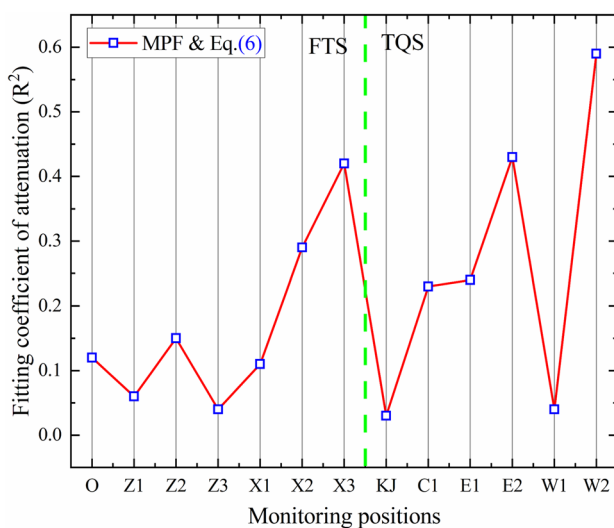
4.3 Combination of PPV and DF for Ground Motions

4.3.1 Evaluation of Damage Potential by Using Currently Safety Standards

To date, many existing vibration standards and criteria are defined by combining both PPV and frequency of blasts, as shown in Fig. 1a, where the limits are based on 2–4 different building types for USBM, DIN, and Chinese standards, respectively, while the building type is not mentioned in OSMRE. To evaluate the measured data, the three most widely used criteria, USBM, OSMRE, DIN 4150, and Chinese standards, are employed and shown in Fig. 19a.

Figure 19a shows that most of the data fall within the acceptable range, while some data exceed the threshold curves outlined in DIN 4150 and the Chinese safety standard. However, as the experimental mine employs a bottom-up mining sequence from − 800 m to a shallow depth, there is a growing necessity for blast vibration control measures to ensure compliance with safety standards.

4.3.2 Response Spectral Analysis of Ground Vibrations

Due to the significant influence of site geology, wave components and other potential factors, attenuation equations cannot perfectly predict either PPV or frequency of ground motions. Thus, the simple combination of PPV and DF is demonstrated in blast vibration safety standards. However, this method only allows us to assess measured vibration data and cannot predict the ground motion. While the goal of thorough ground motion analysis is to prevent potential damage or hazard to surrounding structures in addition to human comfort. Therefore, the response spectrum is utilized to explain ground motions as shown in Fig. 19b, the pseudo-velocity response spectra (PVRS) captured inside rock at different depths from a single-delay shot are also included for comparison. The upward slope on the left primarily reflects the low-frequency portion and response displacement, while the right downward slope reflects the variable high-frequency portion and response acceleration.

Figure 19b illustrates that the spectral amplitudes for inside rock vibration decrease as the direct distance R increases, regardless of acceleration (angle 45°), pseudo-velocity, and displacement (angle 135°). The corresponding DF also shows a decreasing trend from 1700 to 125 Hz. As the vibrations propagate from the bedrock (at a depth of − 140 m) to the ground position KJ (elevation + 37 m) as the black solid curve, the DF decreases significantly from 125 to 15 Hz, while the pseudo-velocity increases from 1.179 mm/s to 1.232 mm/s. This results in a remarkable decline in acceleration and an increase in pseudo displacement, while the ground velocities do not necessarily decrease from inside
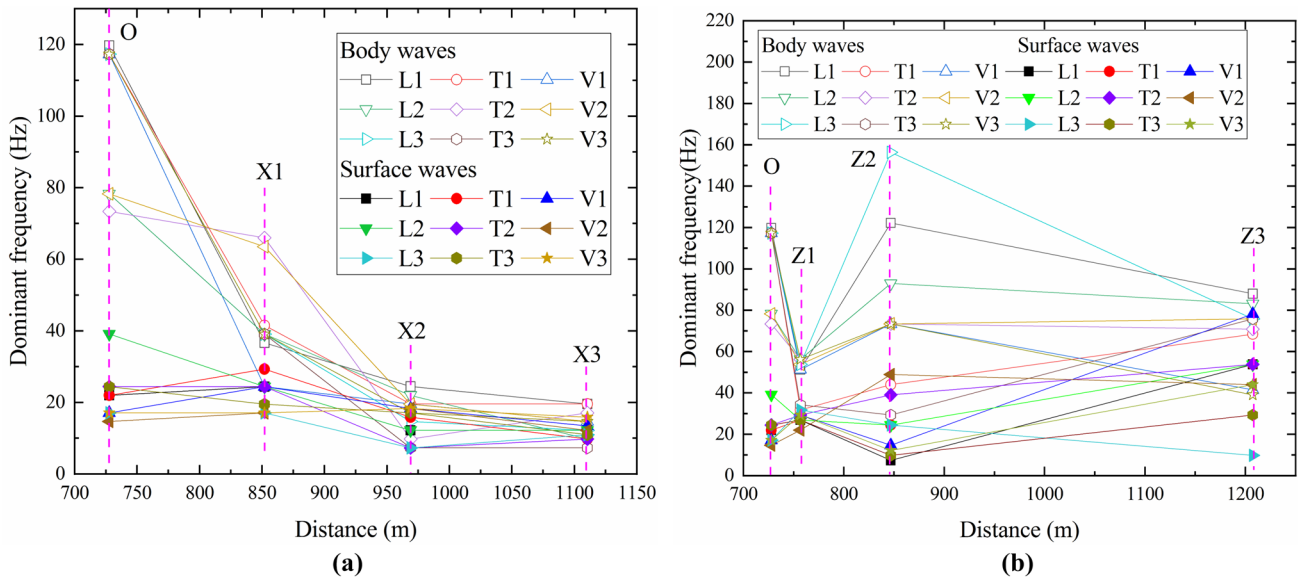

Fig. 17 Fitting coefficients of frequency attenuation at each position using Eq. (6)

Fig. 18 DFs of body waves and surface waves along monitoring lines X (**a**) and Z (**b**), respectively
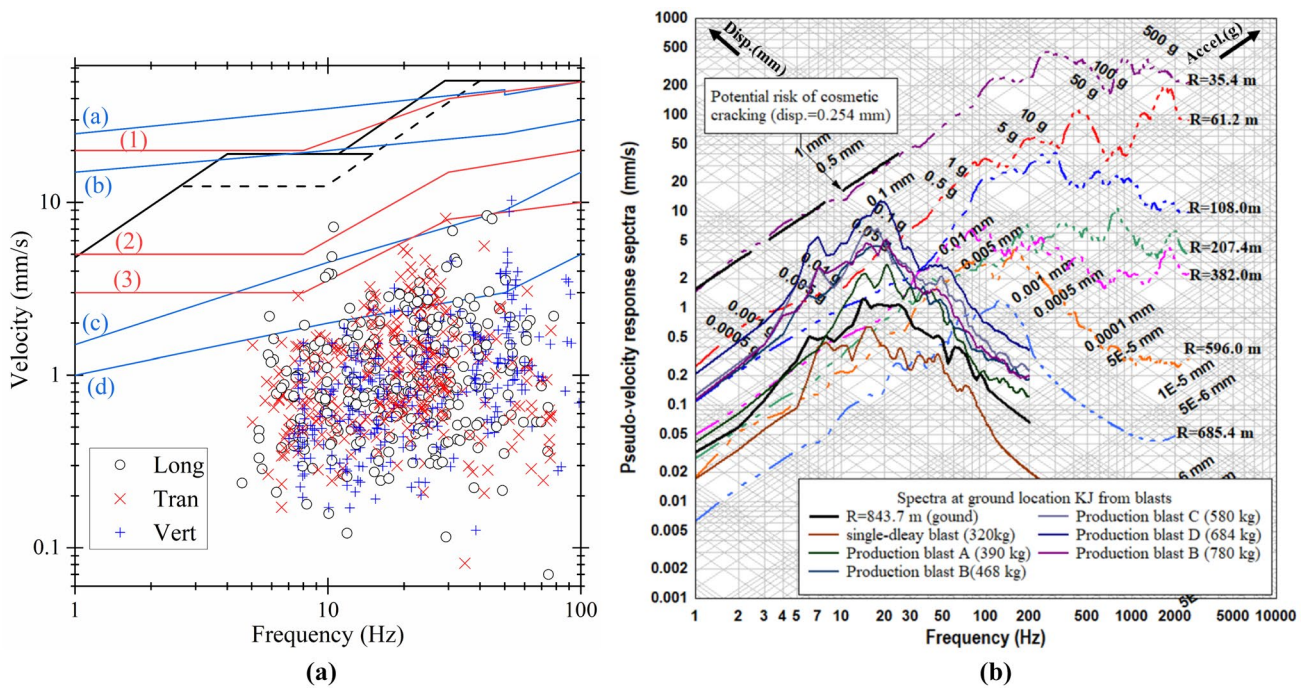

Fig. 19 a The safety standards utilized and the data measured in three components; **b** Response spectra of the V component from inside rock to the ground surface at TQS. Note that the double dot dash in **b** corresponds to vibrations inside rock at varying depths, the single-delay and production shots at position KJ are plotted on the ground surface due to the minimum horizontal projection distance to the inside monitoring positions; the legend for each case provides the maximum charge weight per delay

rock. Dowding (1996) proposed that response displacement plays a critical role in the behavior of ground structures, with a cosmetic cracking criterion of 0.254 mm. Therefore, a significant decrease in ground frequencies adversely affects structures.

In contrast, the response spectra at ground position KJ from single-delay shots and production blasts, show a slight variation in the DFs and shapes of the PVRS, but the pseudo velocity fluctuates within a certain amplitude range. This implies that the response spectra obtained at a designed

ground position would exhibit a similar response shape and DF. However, the similar response behavior at a specific position KJ may be a coincidence. Therefore, the two typical positions O and Z2 at FTS are further selected to analyze the PVRS from the same blasts, which included 3 single-delay shots and 10 production shots. The results are shown in Fig. 20a, b, e, f. The horizontal (combined L and T) and V components are discussed separately due to their different dominant wave components.

At outcrop position O, Fig. 20a, b, reveals that similar PVRSs are observed for either 3 single-delay shots or 10 production blasts, despite the different amplitudes and PVRS shapes of both components. Three single-delay shots produce higher order frequency peaks due to their body wave components and the absence of wave superposition. Furthermore, Fig. 20a indicates that the response velocity amplitudes are proportional to the ground PPVs. For instance, case D, which has a minimum amplitude of 0.64 mm/s, is situated at the base, whereas case J, which has a maximum amplitude of 3.09 mm/s, is at the top. These similarities are also observed at position Z2 with near-surface low-velocity layers, as shown in Fig. 20e, f, although the spectral curve difference decreases between single-delay and production blasts. Therefore, the PVRS exhibit similarity at a designed position for either single-delay shots or production blasts at

the ground surface, irrespective of they are on outcropping rock or on lower propagation layers.

5 New Prediction Method Based on the NPVRS for Ground Motions

5.1 Establishment and Analyses of the NPVRS Method

The above analyses of PPV, frequency, and their combination for ground motions induced by underground blasting reveal many unsolved issues in predicting ground vibrations. Fortunately, the shapes and DFs of the PVRSs are similar at a given ground monitoring position, despite the varied velocity amplitudes. Since the amplitude is basically proportional to the PPV, the normalized pseudo velocity response spectra (NPVRS), defined as the ratio of the PVRS to the ground motion PPV, are plotted for two positions in Fig. 20c, d, g, h, and the NPVRS can denote the magnification of site geologies.

At position O, Fig. 20c, d shows that these NPVRSs tend to be the same, especially in the left upslope, with the exception of three single-delay shots. It is noteworthy that the left uphill slope and its corresponding response displacement is of most concern, since the natural frequencies of buildings
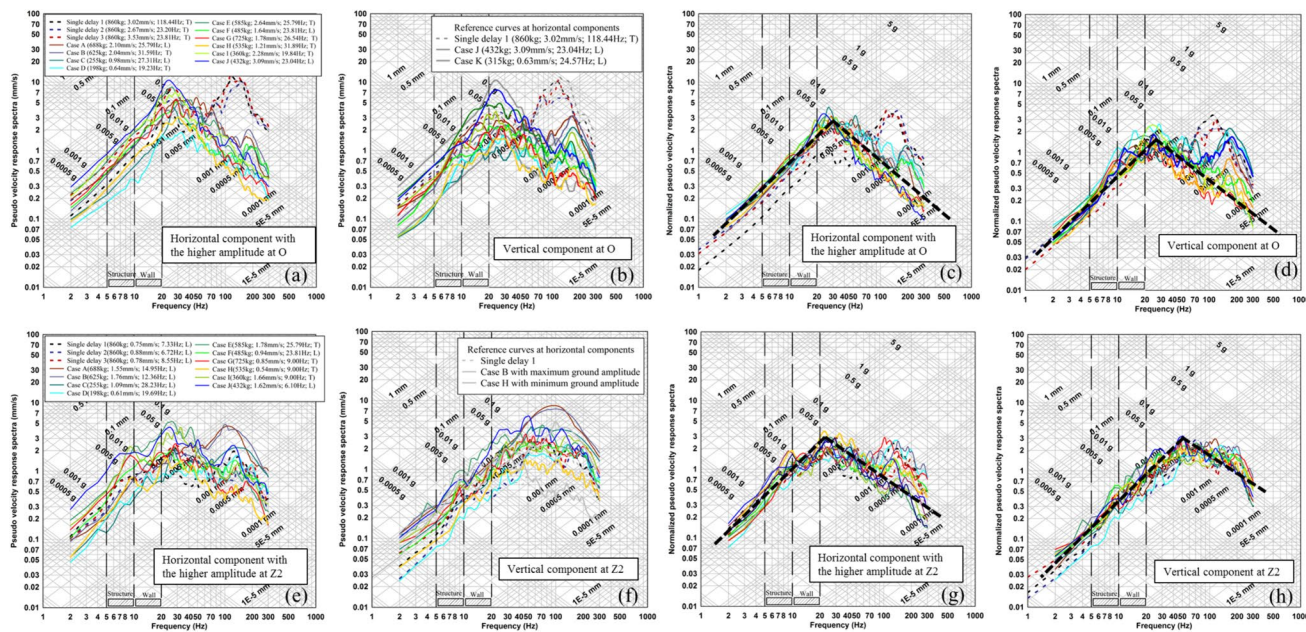

Fig. 20 PVRS and normalized pseudo velocity response spectra (NPVRS) at positions O and Z2 in the horizontal and vertical components, respectively. **a** The PVRS for the horizontal component at O; **b** the PVRS for the vertical component at O; **c** the NPVRS corresponds to (**a**); **d** the NPVRS corresponds to (**b**); **e** the PVRS for the horizontal component at Z2; **f** the PVRS for the vertical component at Z2; **g** the NPVRS corresponds to (**e**); **h** the NPVRS corresponds to (**f**). Note that each curve color corresponds to a specific blast, and the figures are set to the same scale, damping is 5%. The legend provides the maximum charge weight per delay, PPV, DF, and component label for each case

are usually in the range of 5 to 20 Hz (marked in Fig. 20). Thus, the NPVRS can be considered constant and simplified as line segments at specific positions for single-delay shots or multiple-delay blasts. The NPVRS of uphill slopes can also be simplified into a straight line at position Z2, as shown in Fig. 20g, h. This indicates that the NPVRS can accurately reflect the relationship between ground PPVs and response spectra. However, the mathematical correlation between PPVs and response spectra cannot be accurately captured by observing only 10 measured data. Therefore, all available data at both positions are utilized to establish a reliable relationship. Based on the concerning frequency of structures and walls ranging from 5 to 20 Hz and located primarily on the upward slope, Fig. 21 illustrates the relationship between ground PPVs and average relative displacement at positions O and Z2 with the same range.

Figure 21 shows that the relative displacement is linearly proportional to the ground peak amplitudes with a high R^2, while the correlation slopes are distinct for diverse components and positions. Thus, the amplification ratio of the response relative displacement to the ground velocity amplitude varies with different components and positions. Furthermore, the comparison of both components reveals that the blasts produce larger vertical relative displacements in contrast to the horizontal component at outcrop O. However, the horizontal relative displacements exceed those of the vertical component due to site amplification effects at Z2 on near-surface lower propagation layers. This indicates that the ratio of relative displacement of horizontal component

to vertical component could also reflect site geological conditions.

The similar performance of the components allows for the NPVRS to be plotted for one shot at each position. Therefore, Fig. 22a plots the NPVRSs at seven positions of the FTS from the same single-delay shot to observe their differences. Notably, the horizontal component is listed due to its higher amplitudes compared to the vertical component. On the other hand, position X3/E1 is used to confirm whether underground blasting from anywhere (either FTS or TQS) produces the proximity of NPVRS on the same site geological condition. The corresponding NPVRSs are displayed in Fig. 22b.

Figure 22a shows that the NPVRSs vary with position within the same blast, regardless of upward or downward slopes. This indicates that different geologic conditions relevant to ground positions would generate different NPVRSs, and the structural response amplification factors range from 2 to 4 due to the horizontal magnification of site geologic conditions. On the other hand, as shown in Fig. 22b, blasts from distinct ore blocks demonstrate varied spectral performances at the same location, especially in the frequency range of 5–20 Hz. Despite resembling blue and red curves for FTS and TQS blasts, respectively, the proximity of NPVRSs for different ore block blasts is not suggested due to varying propagation paths.
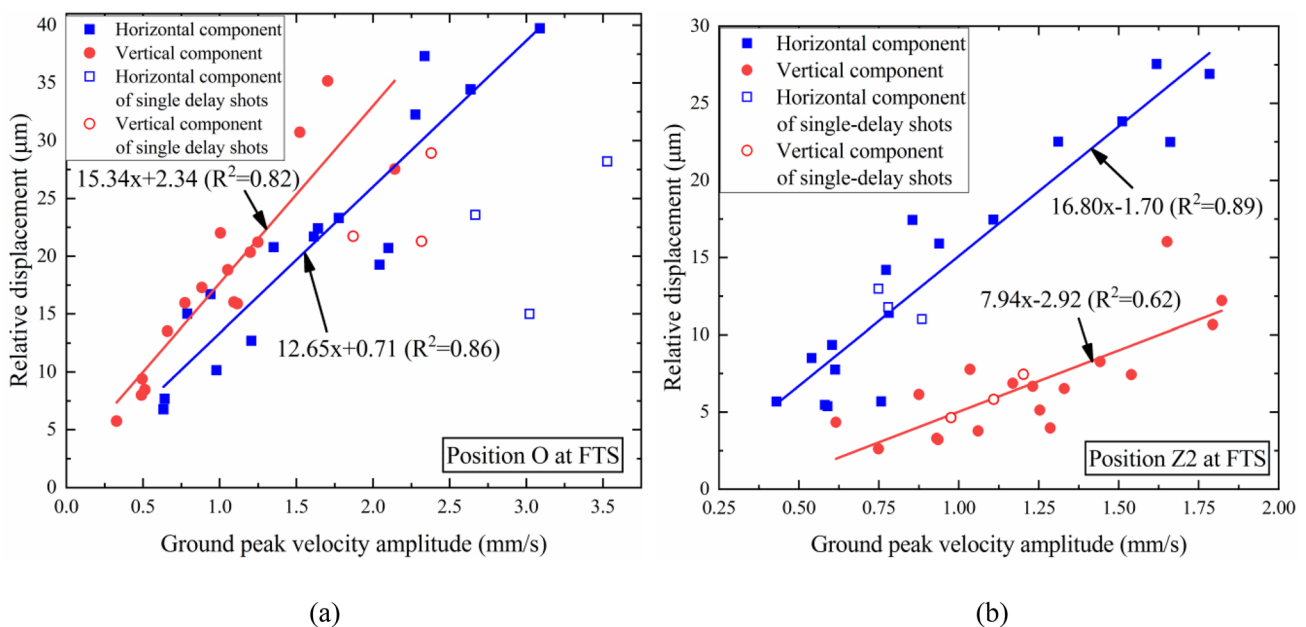

(a)   (b)

Fig. 21 Relationship between ground peak velocity amplitude and average relative displacement over a frequency range of 5–20 Hz at positions O (**a**) and Z2 (**b**). Note that the fitted regressions exclude the scattered single-delay blasting data
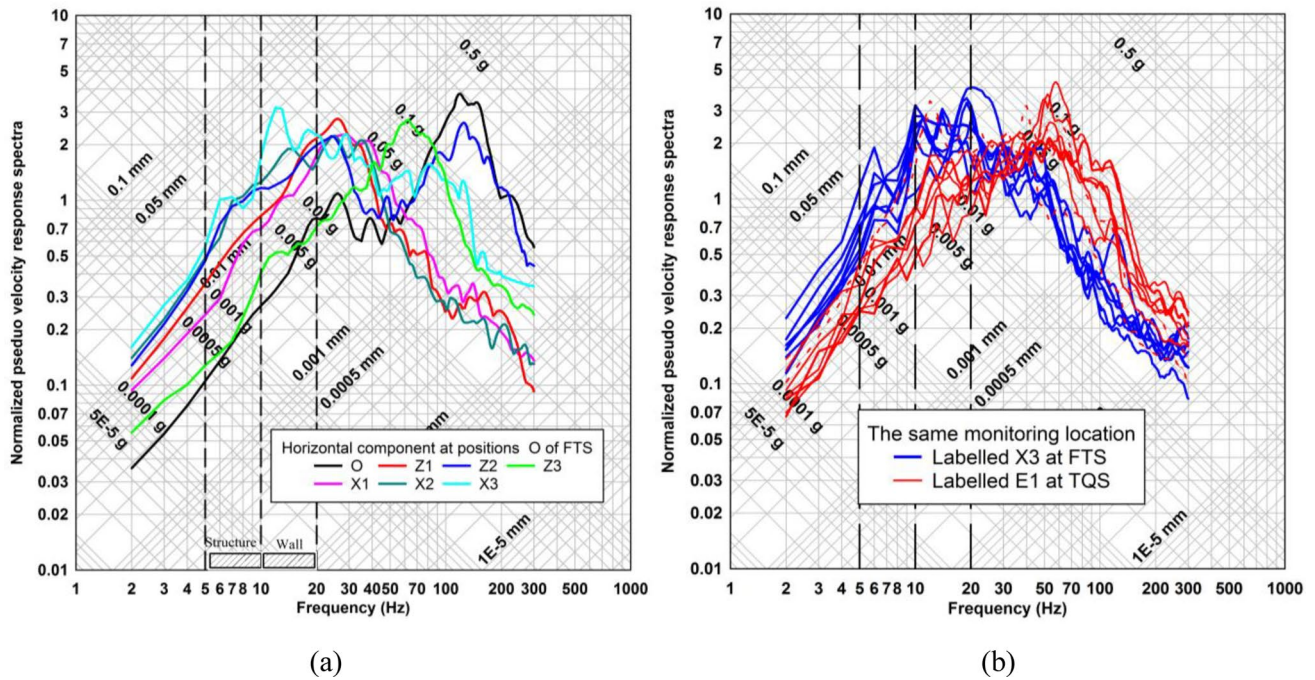
(a)

(b)

Fig. 22 **a** The NPVRSs for the horizontal component at different positions of the FTS from a single-delay shot; **b** The NPVRSs at the same ground position induced by blasts from both ore blocks

5.2 Simple Ground Motion Safety Evaluation Using the NPRVS

The above analyses state that the response spectrum of any ground motion depends not only on the NPVRS, but also on the ground motion amplitudes or PPV. However, it is challenging to predict ground motion PPVs due to various influential factors. Fortunately, the potential damage to buildings is mainly associated with the maximum relative displacements in the 5–20 Hz frequency band, which have a positive correlation with the ground PPVs. Thus, predicting the possible maximum PPV, which represents the upper limit of the regression, is crucial for ground motions. This can be easily obtained from limited measured data. Consequently, the evaluation of ground motions requires only the possible maximum PPV and a NPVRS curve that can be derived from one blast record. For instance, the safety evaluation is performed for the measured FTS ground vibrations with the maximum PPVs, as shown in Fig. 23. It states that the blasts at FTS cannot cause any potential risk of cosmic cracking on ground structures and walls. The velocity spectra at TQS with the maximum PPVs are lower than those at FTS, so they are not listed here.

Based on the given NPVRS curves, the allowable ground velocity amplitude and corresponding frequency at each position also can be illustrated in Table 5. It shows that the relatively low velocity would easily lead to cosmic cracking along the X line at FTS and at positions C1 and E1 at
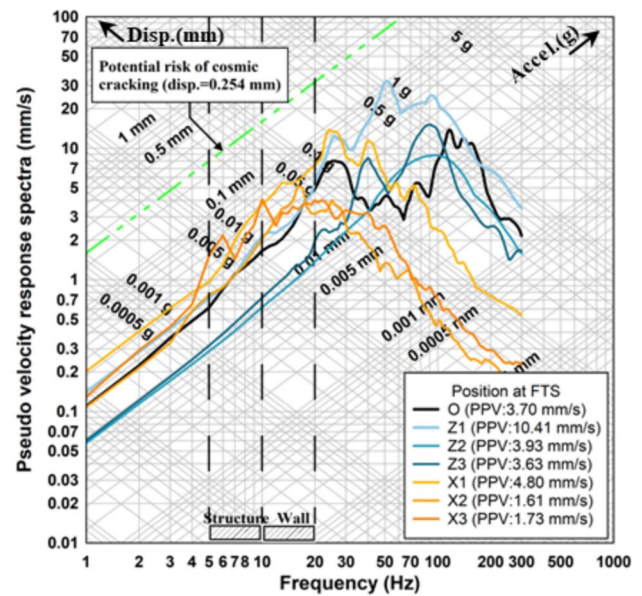

Fig. 23 Response spectra of the Max PPV at each position at FTS

TQS. The TQS vibration induces a relatively low response frequency, and most positions would produce cosmic cracks in the walls. The above analyses demonstrate that the implementation of this method can simplify various potential factors in the vibration prediction process, it also greatly reduces the required monitoring effort for ground vibration

Table 5 Permissible ground velocity and frequency at each position

FTS	Permissible velocity (mm/s)	Frequency (Hz)	TQS	Permissible velocity (mm/s)	Frequency (Hz)
O	23	20	KJ	25	10
Z1	57	20	C1	11	18
Z2	88	20	C2	22	9
Z3	55	19	E1	12	12
X1	18	13	E2	35	11
X2	8	16	W1	26	9
X3	7	10	W2	28	7

assessment, and quickly provides guidance for vibration control. Undoubtedly, it not only gives the site amplification, but also directly reflects the response displacement associated with ground structures and walls.

6 Discussion

Due to the complex characteristics and lack of prediction methods for ground vibration induced by underground blasts, numerical calculations and field experiments with monitoring work were conducted to illustrate the wave propagation characteristics and predict ground vibration. The results show that the wave propagation and attenuation characteristics of ground vibration are intricate, with geological conditions and wave components exerting a significant influence. The numerical method can provide insight into why certain ground amplitudes are higher than those at position KJ inside rock, and why the PPVs at outcrop positions O and OT are scattered or abnormally lower compared to other positions. However, the numerical method only describes wave propagation using a simple 2D model, and the given properties may produce results that are unreliable and do not accurately account for frequency variation and other potential factors.

The difference of ground vibration characteristics induced by open-pit and underground blasts is always concentrated. Upon examining the wave propagation of both blast types, the wavefront induced by open-pit blasts forms cylindrical waves at a certain depth, while the wavefront of underground blasts can be viewed as spherical waves before hitting the ground surface and becomes more complex along the ground surface. The power factor(n) in the scaling attenuation equation is less than 1/3 (it can be 1/6) for underground blasts, while the n is generally accepted to be 1/2 for open-pit blasts. The diverse paths of wave propagation and vibration transformation within geological conditions to the ground surface also create different performance between open-pit

and underground blasts. On the other hand, when comparing the ground vibration with the vibration inside rock induced by underground blasts, it is evident that the amplitude attenuates normally, whereas the frequency experiences a significant drop. The power factor for ground vibration also decreases, while both MPF attenuation can be expressed by the same equation. From rock interior to the ground surface, there is a possibility of an increase in velocity amplitude due to site amplification effects, rather than a necessary decline.

Prediction of ground motions induced by underground blasting is essential to prevent potential damage to nearby structures. However, only PPV or frequency is undesirable to predict the attenuation of ground motions, especially under the significant influence of unaccounted factors, regardless of the overall trend, individual position, or wave components. Besides, the vector peak particle velocity (VPPV) is not employed because our previous work indicates that there is a linear positive correlation between PPV and VPPV (Gou et al. 2020). The simple combination of PPV and DF also falls short of predicting ground motion as it relies on measured data. Since the assessment of potential damage or cracks on structures is the ultimate goal to control ground motions, an appropriate prediction method based on the NPVRS is proposed. The NPVRS not only reflects the site amplification, but also can be simplified to the average relative displacement between 5 and 20 Hz. This relative displacement produces strains that cause cosmetic cracking. The linear correlation between PPV and relative displacement states that controlling the maximum ground amplitudes or PPV can effectively reduce the potential risk to structures. The horizontal components play a critical role in controlling the lateral sway response of the structures.

Maximum ground PPVs are critical for analyzing structural responses and mitigating potential damage. However, there is still uncertainty regarding the key parameters of blast design and geologic medium for determining ground PPVs and frequencies, and more mechanistic research is necessary to explain the weakening effect of charge weight on ground vibration. Further, traditional attenuation equations are not effective in achieving this goal. Systematic work is also needed to evaluate other possible factors associated with the NPVRS of ground motions at a particular position.

7 Conclusions

Ground motions induced by underground mining blasts were investigated by numerical calculations and field experiments. Wave propagation characteristics were illustrated through numerical calculations in comparison with open-pit blasts, then field experiments and recorded vibrations were used to predict ground motions in comparison with

inside rock vibrations. Relying only on PPV, frequency, and the simple combination of PPV and DF is undesirable for predicting ground motions, a novel prediction method is proposed based on normalized pseudo-velocity response spectra (NPVRS). The main conclusions are as follows:

1. Diverse paths of wave propagation and vibration transformation to the ground surface produce different performance between open-pit and underground blasting. The ground amplitude induced by underground blasting attenuates relatively slower with the decreasing effect of charge weight, the corresponding power factor in the scaling attenuation equation is less than 1/3 or 1/2, it could be 1/6.
2. Compared ground motions to inside rock vibration induced by underground blasting, the amplitude attenuates normally while the frequency drops significantly. The effect of charge weight on ground PPVs decreases as the damping effect of the propagating material increases. The mean power frequency (MPF) is significantly better than the DF to describe the frequency attenuation.
3. The NPVRS can be simplified as line segments at specific positions for single-delay or multiple-delay blasts; the relative displacement in the concerning frequency range of 5–20 Hz is linearly proportional to the ground PPVs. The allowable ground velocity amplitude and frequency at each position can be derived from the possible maximum PPV and a NPVRS curve from one blast record.
4. The NPVRS method not only gives the site amplification, but also directly reflects the response displacement associated with cosmetic cracking and damage to the structure. It greatly simplifies various potential factors and reduces the required monitoring effort in vibration prediction and evaluation.
5. Geology primarily impacts the ground PPV levels rather than its attenuation rates, site geological conditions

amplify amplitudes in the horizontal components (especially under the condition of gradually decreasing layer properties) and greatly affect the body wave frequencies. The horizontal component of the ground vibration is more sensitive to the charge weight and has a slower attenuation rate than the vertical component.

Appendix

A: Dimensionless Frequency Attenuation Equation

Frequencies of blast-induced ground motions are affected by various factors, and they are listed in Table 6.

According to the π-theorem, W, R, C_S were chosen as the basic physical quantities. Provided that π is on behalf of the dimensionless group, the composite formula of π is shown as follows

$$\pi = W^{a_1}R^{b_1}C_S^{c_1}f \tag{7}$$

According to the dimensions in Table 6, the simplified equations are shown as follows.

$$\pi_1 = Rf/C_S, \ \pi_2 = C_S/D, \ \pi_3 = f\Delta t, \\ \pi_4 = R^3\rho_m/W, \ \pi_5 = R^3/WC_s^2, \tag{8}$$

Based on the equation of similar dimensionless group can be written as

$$\pi_1 = \phi(\pi_5) \tag{9}$$

That is,

$$fR/C_s = \phi(R^3/WC_s^2) \tag{10}$$

Or

Table 6 Factors associated with surface ground motions

Variable		Symbol	Unit	Dimension
Explosion conditions	Charge weight per delay	W	kg	M
	Velocity of detonation (VOD)	D	m/s	L/T
	Burden/spacing	B/S	m	L
	Delay time	Δt	ms	T
Propagating medium	Density of rock or soil	ρ_m	Kg/m³	M/L³
	Shear velocity of rock/soil along travel path	C_S	m/s	L/T
	Distance from the source	R	m	L
	Elastic modulus	E	Pa (N/m²)	M/(T²L)
	Poisson's ratio	v	-	1
	Peak particle velocity	PPV	m/s	L/T
	Frequency of the ground motion	f	Hz	1/T

$$f = k\frac{C_S}{R}\left(R^3/W\right)^\alpha \tag{11}$$

Eq. (11) can be converted to

$$f = kC_S W^{-1/3}\left(R^3/W\right)^{\alpha-1/3} \tag{12}$$

Based on shear velocity item C_S and k are unknown, Eq. (12) can be converted as

$$\ln fW^{1/3} = \ln K + \alpha\prime\ln\left(R/W^{1/3}\right) \tag{13}$$

Data availability Data will be made available on request.

Declarations

Conflict of interest The authors declare that they have no known competing financial interests or personal relationships that could have appeared to influence the work reported in this paper.

References

Ainalis D, Kaufmann O, Tshibangu J-P et al (2016) Modelling the source of blasting for the numerical simulation of blast-induced ground vibrations: a review. Rock Mech Rock Eng 50:171–193. https://doi.org/10.1007/s00603-016-1101-2

Blair DP (1990) A direct comparison between vibrational resonance and pulse transmission data for assessment of seismic attenuation in rock. Geophysics 55:51–60

Blair DP (2004) Charge weight scaling laws and the superposition of blast vibration waves. Fragblast 8:221–239

Blair DP (2007) A comparison of Heelan and exact solutions for seismic radiation from a short cylindrical charge. Geophysics 72:E33–E41

Blair DP (2015a) The free surface influence on blast vibration. Int J Rock Mech Min Sci 77:182–191

Blair DP (2015b) Wall control blasting. In: Proceedings of the 11th international symposium on rock fragmentation by blasting. pp 13–26

Blair DP (2020) Approximate models of blast vibration in non-isotropic rock masses. Int J Rock Mech Min Sci 128:104245. https://doi.org/10.1016/j.ijrmms.2020.104245

Blair DP (2023) Blast vibration in layered coal strata : measurements , analysis and modelling. In: European federation of explosives engineers. pp 201–216

Dai DH, Zhang N, Lee VW et al (2019) Scattering and amplification of SV waves by a semi-cylindrical hill in a half-space by a wavefunction-based meshless method using mapping and point-matching strategies. Eng Anal Bound Elem 106:252–263. https://doi.org/10.1016/j.enganabound.2019.05.016

Dearman WR (1995) Description and classification of weathered rocks for engineering purposes: the background to the BS5930: 1981 proposals. Q J Eng Geol Hydrogeol 28:267–276

Dogan O, Anil Ö, Akbas SO et al (2013) Evaluation of blast-induced ground vibration effects in a new residential zone. Soil Dyn Earthq Eng 50:168–181. https://doi.org/10.1016/j.soildyn.2013.03.005

Dowding CH (1996) Construction vibrations. Prentice Hall Upper Saddle River, NJ

Gharehdash S, Sainsbury BAL, Barzegar M et al (2021) Field scale modelling of explosion-generated crack densities in granitic rocks using dual-support smoothed particle hydrodynamics (DS-SPH). Rock Mech Rock Eng 54:4419–4454

Gharehgheshlagh HH, Alipour A (2020) Ground vibration due to blasting in dam and hydropower projects. Rud Geol Naft Zb 35:59–66. https://doi.org/10.17794/rgn.2020.3.6

Görgülü K, Arpaz E, Demirci A et al (2013) Investigation of blast-induced ground vibrations in the Tülü boron open pit mine. Bull Eng Geol Environ 72:555–564

Gou YG, Shi XZ, Yu Z et al (2023) Evaluation of underground blast-induced ground motions through near-surface low-velocity geological layers. J Rock Mech Geotech Eng 15:600–617

Gou YG, Shi XZ, Zhou J et al (2020) Attenuation assessment of blast-induced vibrations derived from an underground mine. Int J Rock Mech Min Sci. https://doi.org/10.1016/j.ijrmms.2020.104220

Gui YL, Zhao ZY, Jayasinghe LB et al (2018) Blast wave induced spatial variation of ground vibration considering field geological conditions. Int J Rock Mech Min Sci 101:63–68. https://doi.org/10.1016/j.ijrmms.2017.11.016

Hallquist JO (2006) LS-DYNA theory manual. Livermore Softw Technol Corp 3:25–31

Hao H, Wu YK, Ma GW, Zhou YX (2001) Characteristics of surface ground motions induced by blasts in jointed rock mass. Soil Dyn Earthq Eng 21:85–98

Hong ZX, Tao M, Wu CQ et al (2023) The spatial distribution of excavation damaged zone around underground roadways during blasting excavation. Bull Eng Geol Environ. https://doi.org/10.1007/s10064-023-03114-6

Ietto F, Perri F, Cella F (2018) Weathering characterization for landslides modeling in granitoid rock masses of the Capo Vaticano promontory (Calabria, Italy). Landslides 15:43–62

Jayasinghe B, Zhao ZY, Chee AGT et al (2019) Attenuation of rock blasting induced ground vibration in rock-soil interface. J Rock Mech Geotech Eng 11:770–778

Jedele LP (2012) Energy-Attenuation Relationships from Vibrations Revisited. Soil Dyn Symp Honor Profr Richard D Woods 1–14

Jiang N, Zhou CB, Lu SW, Zhang Z (2017) Propagation and prediction of blasting vibration on slope in an open pit during underground mining. Tunn Undergr Sp Technol 70:409–421. https://doi.org/10.1016/j.tust.2017.09.005

Karadogan A, Kahriman A, Ozer U (2014) A new damage criteria norm for blast-induced ground vibrations in Turkey. Arab J Geosci 7:1617–1626. https://doi.org/10.1007/s12517-013-0830-8

Kuhlmeyer RL, Lysmer J (1973) Finite element method accuracy for wave propagation problems. ASCE Soil Mech Found Div J 99:421–427

Kumar R, Choudhury D, Bhargava K (2016) Determination of blast-induced ground vibration equations for rocks using mechanical and geological properties. J Rock Mech Geotech Eng 8:341–349. https://doi.org/10.1016/j.jrmge.2015.10.009

Kumar S, Mishra AK, Choudhary BS et al (2020) Prediction of ground vibration induced due to single hole blast using explicit dynamics. Mining, Metall Explor 37:733–741. https://doi.org/10.1007/s42461-019-00162-z

Li JC, Ma GW, Zhou YX (2011) Analytical study of underground explosion-induced ground motion. Rock Mech Rock Eng 45:1037–1046. https://doi.org/10.1007/s00603-011-0200-3

Liu QJ, Zhao MJ, Wang LH (2013) Scattering of plane P, SV or Rayleigh waves by a shallow lined tunnel in an elastic half space. Soil Dyn Earthq Eng 49:52–63. https://doi.org/10.1016/j.soildyn.2013.02.007

Liu D, Lu WB, Yang JH et al (2022) Relationship between cracked-zone radius and dominant frequency of vibration in tunnel blasting. Int J Rock Mech Min Sci 160:105249. https://doi.org/10.1016/j.ijrmms.2022.105249

Lu WB, Luo Y, Chen M, Shu DQ (2012) An introduction to Chinese safety regulations for blasting vibration. Environ Earth Sci 67:1951–1959

Lv JL, Liu Z, Huang JH (2023) The vibration propagation and damage distribution characteristics of deep-buried underground cavern blasting. Mech Time-Dependent Mater. https://doi.org/10.1007/s11043-023-09615-x

Ray S, Dauji S (2019) Ground vibration attenuation relationship for underground blast: a case study. J Inst Eng Ser A 100:763–775. https://doi.org/10.1007/s40030-019-00382-y

Rouse N, Schnell D, Worsey T (2020) Regression Model for Surface Vibrations from Underground operations. In: Proceedings of the 46th annual conference on explosives and blasting technique. International Society of Explosives Engineers, Denver, Colorado, USA, pp 1–10

Roy MP, Singh PK, Sarim M, Shekhawat LS (2016) Blast design and vibration control at an underground metal mine for the safety of surface structures. Int J Rock Mech Min Sci 83:107–115. https://doi.org/10.1016/j.ijrmms.2016.01.003

Tribe J, Koroznikova L, Khandelwal M, Giri J (2021) Evaluation and assessment of blast-induced ground vibrations in an underground gold mine: a case study. Nat Resour Res 30:4673–4694. https://doi.org/10.1007/s11053-021-09943-0

Venkatesh HS (2005) Influence of total charge in a blast on the intensity of ground vibrations—field experiment and computer simulation. Fragblast 9:127–138

Wang HL, Zhao Y, Shan RL et al (2023) Safety evaluation and application of blasting vibration based on an improved hilbert-huang transform. Rock Mech Rock Eng 56:3971–3991. https://doi.org/10.1007/s00603-023-03272-9

Wu CQ, Hao H (2005) Numerical study of characteristics of underground blast induced surface ground motion and their effect on aboveground structures. Part I. Ground motion characteristics. Soil Dyn Earthq Eng 25:27–38. https://doi.org/10.1016/j.soildyn.2004.08.001

Yaghmaei-Sabegh S, Rupakhety R (2020) A new method of seismic site classification using HVSR curves: a case study of the 12 November 2017 Mw 7.3 Ezgeleh earthquake in Iran. Eng Geol 270:105574. https://doi.org/10.1016/j.enggeo.2020.105574

Yan Y, Hou XM, Fei HL (2020) Review of predicting the blast-induced ground vibrations to reduce impacts on ambient urban communities. J Clean Prod 260:121135. https://doi.org/10.1016/j.jclepro.2020.121135

Yang JH, Cai JY, Yao C et al (2019) Comparative study of tunnel blast-induced vibration on tunnel surfaces and inside surrounding rock. Rock Mech Rock Eng 52:4747–4761. https://doi.org/10.1007/s00603-019-01875-9